REDUCTION OF DISCRETE AND FINITE ELEMENT MODELS USING BOUNDARY CHARACTERISTIC ORTHOGONAL VECTORS

Raghdan Joseph Al Khoury

A Thesis in

The Department of

Mechanical and Industrial Engineering

Presented in Partial Fulfillment of the Requirements for the

Degree of Master of Applied Science (mechanical engineering)

Concordia University

Montreal, Québec

Canada

August 2008

Your file Votre référence
ISBN: 978-0-494-45450-3
Our file Notre référence
ISBN: 978-0-494-45450-3

ABSTRACT

REDUCTION OF DISCRETE AND FINITE ELEMENT MODELS USING BOUNDARY CHARACTERISTIC ORTHOGONAL VECTORS

Raghdan Joseph Al Khoury

Solution of large eigenvalue problems is time consuming. Large eigenvalue problems of discrete models can occur in many cases, especially in Finite Element analysis of structures with large number of degrees of freedom. Many studies have proposed reduction of the size of eigenvalue problems which are quite well known today.

In the current study a survey of the existing model reduction methods is presented. A new proposed method is formulated and compared with the earlier studies, namely, static and dynamic condensation methods which are presented in detail. Many case studies are presented.

The proposed model reduction method is based on the boundary characteristic orthogonal polynomials in the Rayleigh-Ritz method. This method is extended to discrete models and the admissible functions are replaced by vectors. Gram-Schmidt orthogonalization was used in the first case study to generate the orthogonal vectors in order to reduce a building model.

Further, a more general method is presented and it is mainly used to reduce FEM models. Results have shown many advantages for the new method.

À JINA, JOSEPH, ALAA ET SAMI

Acknowledgments

I would like to express my gratitude towards my supervisor, Professor Rama B. Bhat for his guidance and valuable advice. He was always a great help in the process of developing my thesis.

I would also like to acknowledge Dr. A. K. Waisuddin Ahmed for his guidance in the beginning of my studies at Concordia University.

My gratitude must also go to Joe Hulet for always aiding me with my technological problems. Finally, I would like to thank all my colleagues, especially my lab mates for the beneficial discussions that we held and for the good times I experienced.

Table of Contents

List of Figures

List of Tables

Nomenclature

$\{\phi_i\}$	Normalized assumed deflection vector
$\{\hat{\phi}_i\}$	Non normalized assumed deflection vector
$[M]$	Mass Matrix
$[K]$	Stiffness Matrix
$[C]$	Damping Matrix
x_b	Base excitation
$\{s\}$	Uniform load vector
M_i	Mass of i^{th} DOF
k_i	Stiffness coefficient of i^{th} spring
c_i	Damping coefficient of i^{th} spring
$\{x\}$	Deflection vector
$[D]$	Dynamic matrix
$\{F\}$	Force vector
$[D_{mm}]$	Master-master dynamic matrix
$[D_{ms}]$	Master-slave dynamic matrix
$[D_{sm}]$	Slave-master dynamic matrix
$[D_{ss}]$	Slave-slave dynamic matrix
$[x_m]$	Master deflection
$[x_s]$	Slave deflection
$[K_{mm}]$	Master-master Stiffness matrix
$[K_{ms}]$	Master-slave stiffness matrix
$[K_{sm}]$	Slave-master stiffness matrix
$[K_{ss}]$	Slave-slave stiffness matrix
$[M_{dd}]$	Deflection-deflection Mass matrix
$[M_{ds}]$	Deflection-slope mass matrix
$[M_{sd}]$	Slope-deflection mass matrix
$[M_{ss}]$	Slope-slope mass matrix

$[K_{dd}]$	Deflection-deflection Stiffness matrix
$[K_{ds}]$	Deflection-slope stiffness matrix
$[K_{sd}]$	Slope-deflection stiffness matrix
$[K_{ss}]$	Slope-slope stiffness matrix
$\{\varphi_{d,i}\}$	i^{th} deflection vector
$\{\varphi_{s,i}\}$	i^{th} slope vector
$\{q\}$	Generalized coordinate vector
$[T_r]$	Transformation matrix
$w(x,y)$	Deflection function in term of x and y
E	Young modulus
h	Thickness of the plate
ν	Poisson's ratio
ρ	Density
T_{max}	Maximum kinetic energy
U_{max}	Maximum potential energy
q_m	m^{th} generalized coordinate
λ	Non-dimensional eigenvalue
ξ	Non-dimensional abscissa
η	Non-dimensional ordinate

Chapter 1

Introduction

1.1. General information

Real structures and systems can be modeled as either continuous or discrete or a combination of both. The vibration behavior of such structures is studied by expressing the vibratory motion in the form of differential equations that may be solved analytically in some cases or using approximate methods in other. In general, discretization of a continuous structure is a powerful method to solve the differential equations with acceptable accuracy. Two of the well known methods are the Rayleigh-Ritz and the Finite Element Method (FEM).

Briefly, FEM or FEA (finite element analysis) is a numerical method to solve partial differential equations by transforming the problem into a set of ordinary differential equations that can be solved using different numerical methods. FEM was first proposed in 1941 and 1942, in order to solve structural problems. This method has evolved over the years with many improvements and it forms now one of the most used methods to simulate physical systems. This method can be used for the static and dynamic analysis, where a continuous structure is discretized into a finite number of DOFs. Currently, a variety of elements are used for the structural analysis such as: rod, beam, plate, shell and

solid. Most of these elements can be found in the many software packages available today. Many books have been written on this method, such as by Rao [1] and Reddy [2].

The Rayleigh-Ritz method was proposed by Walter Ritz. Similar to FEM, this method is used as a numerical method to solve partial differential equations by discretizing the problem. The Rayleigh-Ritz method uses a set of deflection shapes satisfying at least the geometrical boundary conditions and employs them in the energy expressions [3]. Using the stationarity conditions of the Rayleigh's quotient by differentiating with respect to all the generalized coordinates, results in a set of simultaneous algebric equations that can be solved to obtain the approximate results. The accuracy in this method is better when larger number of assumed modes are employed.

1.2. The Rayleigh Ritz method

The Rayleigh-Ritz method defines the actual deflection shape during vibration as a linear combination of assumed deflection shapes, each of which satisfy at least the geometrical boundary conditions of the structure. The expression for the deflection as a linear combination of the linearly independent assumed deflection shapes $\{\varphi_i\}$ is given as

$$W(x) = \sum_{i=1}^{n} a_i \varphi_i(x) \qquad (1.1)$$

The expressions of the energy can then be written in terms of the assumed deflection. Assuming that the motion is harmonic in one of the system natural frequencies under free vibration conditions, the Rayleigh's quotient will be the ratio of the maximum strain

energy over the maximum kinetic energy. Applying the stationary condition to the natural frequencies by differentiating it with respect to the arbitrary coefficients a_i will lead to a (n × n) eigenvalue problem.

$$\frac{\partial(\omega^2)}{\partial a_i} = \frac{T_{\max}\dfrac{\partial U_{\max}}{\partial a_i} - U_{\max}\dfrac{\partial T_{\max}}{\partial a_i}}{T_{\max}^2} = 0 \qquad (0.2)$$

This method is quite suitable to solve partial differential equations, provided a set of linearly independent assumed deflection functions can be found.

1.2. Boundary characteristic orthogonal polynomials

The Rayleigh-Ritz method has been used to solve different vibration problems. For plate problems admissible functions were chosen as a product of the beam characteristic functions which are the exact mode shapes of beams with the corresponding boundary conditions. This method was used in many studies, mainly to solve for the eigenvalues of plates which have no analytical solutions. Rectangular plates have an exact solution only when two facing edges are simply supported. Also Kirchhoff [4] presented analytical solution of circular plates. Detailed review of plate theory as well as a review of the computational method used to solve it is found in Soedel [5].

Dickinson and Li [6] presented a procedure to solve rectangular plate problem for different boundary conditions by using admissible functions that are based on the arbitrary assumption of two simply supported facing edges and solving for the exact

mode shapes from the resulting ordinary differential equation using actual boundary conditions on the other two edges. This process is repeated to obtain the exact mode shapes between the initial two edges by assuming that the latter two opposite edges are simply supported. Then the plate deflection is assumed as the product of the two sets of exact deflection functions. All the studies listed in [7]-[12] have used either the Rayleigh or the Rayeigh-Ritz method for plate problems with admissible functions taken as the product of exact beam functions.

Bhat [13] proposed a method to generate boundary characteristic orthogonal polynomials (BCOP) as admissible functions in the Rayleigh-Ritz method. This method was used to solve the eigenvalue problem of plates with different boundary conditions. It is based on a first polynomial that satisfies all the boundary conditions while the rest of the functions are generated using Gram-Schmidt orthogonalization method [14]. Note that the functions that form the rest of the set will satisfy only the geometrical boundary conditions.

This BCOPs were used to solve the eigenvalue problem of beams and plates with different boundary conditions and geometry. Tapered beams and plates were studied using a weight function in the construction of the higher members of the set. Nonclassical boundary conditions such as translational springs or spring hinged cases were studied using the polynomials of structures with free ends. Plate problems were solved using the product of one-dimensional polynomials as admissible functions. Moreover functions in polar coordinates were used to study circular and elliptical plate problems.

Grossi and Bhat [15] presented a study where tapered beams were solved using BCOPs generated by adding a weight function to the orthogonalization algorithm. The results were compared with the exact ones given in terms of Bessel functions. Bhat et al [16], studied the case of thin plates with non uniform thickness using the BCOP in the Rayleigh-Ritz method and compared with many other methods namely, the Rayleigh-Ritz method with a tuned parameter, the optimized Kantorovich method [17] and the FEM.

As for the case of nonclassical boundary conditions, the case of an elastic support preventing rotation at one end and an added mass at the second end was studied in [18] by Grossi et al. In this study the first assumed deflection shape is chosen to satisfy only the geometrical homogeneous boundary conditions, which means only one condition in this case. Numerical results were obtained for different cases of linearly tapered beam.

The flexural vibration of polygonal plates was studied using two dimensional polynomials by Bhat [19]. Starting from a function that satisfies the geometrical boundary conditions, the rest of the functions were generated using Gram-Schmidt method and numerical results for the case of triangular plates were presented. Triangular plates also received considerable interest from researchers. The vibration of completely free triangular plate was studied by Leissa and Jaber [20]. Also variable thickness triangular plates were studied by Singh and Saxena [21], using the Rayleigh-Ritz method with boundary characteristic orthogonal polynomials. In this study the polynomials of any triangle are mapped into an isoceles right angle triangle. Liew and Wang [22] studied the cases of triangular plates with point supports or internal point supports with supported edges; in this study the authors used a combination of the Rayleigh-Ritz and Lagrangian

multiplier methods. Many cases of triangular plates with different supports and with internal point supports have been solved. Liew [23] also used boundary characteristic orthogonal polynomials to solve triangular plates with different geometries and boundary conditions. Results in this paper covered a wide range of case studies.

Elliptical and circular plates were studied using a set of functions in polar coordinates. Rajalingham and Bhat [24] studied the axisymmetric vibration of elliptical and circular plates using boundary characteristic orthogonal functions in radial direction. In [25] the same authors used the BCOPs in the radial direction, however, they included the circumferential variation using trigonometric functions. The case of nonuniform elliptical plate was studied by Singh and Chakraverty [26] taking into consideration different kinds of nonuniformity, namely, linear and quadratic either parallel to the major axis or radial through the ellipse.

Bhat [27] used BCOP method as a model reduction technique for the case of a one dimensional finite element model of a rotating shaft. The model reduction method was extended for reducing discrete and FEM [28] models using boundary characteristic vectors. Further, admissible two dimensional functions for plate problems were generated using an orthogonalization technique proposed by Staib [29].

1.3. Model reduction

Model reduction is advised for large eigenvalue problems, especially when only the first few modes are of interest, which is usually the case. Model reduction is useful to

reduce the computational effort, and it can form a very important basis for multi-mode control of complex flexible structures. Moreover, FEM often results in a large number of degrees of freedom, and model reduction is widely used in all structural modal analysis. Basically, the model reduction is used in order to reduce the computational effort needed to solve the eigenvalue problem. Mathematically, solution of the eigenvalue problem is similar to the finding of the roots of polynomials of an order similar to that of the size of the eigenvalue problem. However, simple numerical approaches involving matrix operation have been proposed to find the eigenvalues.

Many methods were based on an iterative process to converge toward the best solution, for example, the subspace iteration and the simultaneous iteration. Many model reduction techniques were studied and reported in the literature. The method that is known by the eigenvalue economization or the static condensation was proposed by Guyan [30] and Irons [31]. The method is based on the elimination of slave degrees of freedom which are chosen along with the master ones. The correct choice of the master degrees of freedom is important in this method since it may cause the loss of few lower modes otherwise. The choice of the master DOF is related to the distribution of energy within the structure. This method uses the static properties of the structure and hence it gives better results for all frequencies close to zero. An improved model reduction method was proposed by O'Callahan [32] where a restriction was applied on the choice of DOF that are to be eliminated and this method showed better results. This method was extended for higher frequencies by Salvini and Vivio [33].

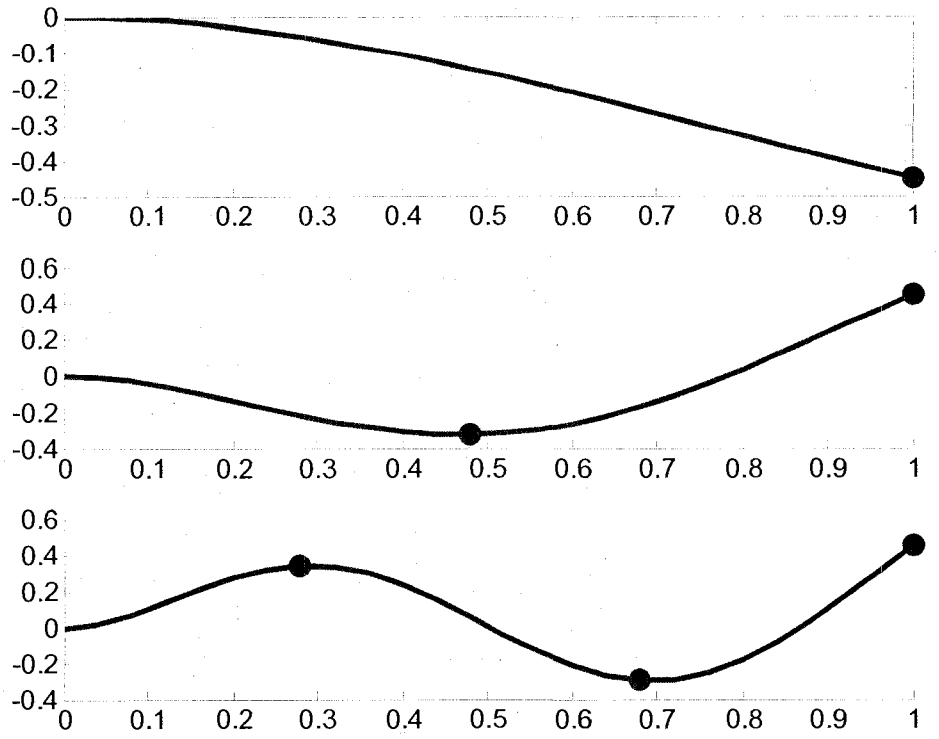

Fig. 1: Master DOF selection in a cantilever beam.

Fig. 1 shows a valid selection of the DOF for three different vibration modes of a cantilever beam. This selection is based on the energy distribution in different modes. As mentioned earlier, a different choice of master DOF may result in the loss of some lower modes.

The exact dynamic condensation was proposed by Leung [34]. This method requires the inverse of the dynamic stiffness matrix at any desired frequency. This method also requires the choice of master and slave DOF. When the method was introduced, only those nodes where the structure is subjected to external excitation were chosen as master DOFs. Myklebust et al [35] have investigated the viability of model reduction methods

with nonlinear dynamic problems. Also the same author in [36] compared the static condensation method or Guyan reduction with the improved reduction model (IRS) and the modal synthesis technique first proposed by Hurty [37] and Craig [38]. Modal synthesis technique, also known as component mode substitution, is based on the assumption of the continuous system as an assembly of subsystems which are solved independently and assembled mathematically [39]. This study has shown a good match between the (IRS) modal synthesis techniques, while the static condensation has shown a larger error. Lanczos vectors have been also used in the dynamic substructure analysis [40]. An iterative method using Lanczos vectors were used to solve eigenvalue problem in [41].

In the present study the model reduction is performed using a set of boundary characteristic orthogonal vectors that satisfy the boundary conditions. These vectors are employed in the Rayleigh-Ritz method in order to reduce the model. These vectors are generated using two different methods one following Bhat [13] and second using Leger, Wilson and Clough [42]. In the latter the generated vectors are load dependent vectors that are calculated as static deflections. Another method that involves the frequency in the calculation of Ritz vectors can is presented by Xia and Humar [43].

In the method by Bhat [13] the procedure was applied to a high-rise building vibration. This method showed the ability of reducing the models with acceptable results. However, this method showed some problems when applied to FEM due to the presence of the dependent degrees of freedom.

The second method of condensation is basically designed for finite Element Models. In this method a set of boundary characteristic vectors are generated following [42]. The importance of this method is that it does not need either modal or physical coordinates in order to generate the set of vectors.

The detailed formulation of static and dynamic condensation is explained in subsequent chapters. Moreover, one can find a good review of those methods and different computational methods in [44] by Meirovitch and [45] by Leung.

1.4. Objectives and scope of the research

The use of boundary characteristic orthogonal polynomialsin the Rayleigh-Ritz method is extended to the study of discrete systems. When the structure is continuous the employed functions will help in discretizing the system. Mathematically, it is used for solving a partial differential equation by transforming it to a set of simultaneous algebric equations. However, when the system is discrete by nature then the application of the Rayleigh-Ritz method will not be necessary for the solution but it may form the basis of a model reduction method depending on the number of employed vectors.

The aim of this thesis is to extend the application of boundary characteristic orthogonal polynomials to discrete systems in which the admissible deflection shape will be expressed in terms of orthogonal vectors. To achieve this goal, a method is proposed to reduce the discrete models using the Gram-Schmidt technique for orthogonalization. Next step is to generalize this method so that it can be applied to all discrete models. The

new proposed reduction technique for FEM models was investigated using many example structures and compared with previous well known reductions methods.

1.6. Organization of the thesis

The thesis contains 6 chapters. These chapters cover the formulation and the examples used to demonstrate the proposed model reduction methods.

The 1st chapter provides an introduction containing a literature review and notions about the FEM and Rayleigh-Ritz methods. It also contains a survey of the earlier studies of model reduction techniques and the use of boundary characteristic orthogonal polynomials in the Rayleigh-Ritz method.

Chapter 2 and 3 are on the reduction of discrete and FEM models using a set of orthogonal vectors that are generated using two different methods. In chapter 2 the orthogonal vectors are generated using Gram-Schmidt method and employed in the Rayleigh-Ritz method to reduce the model of a building. The original model is made of 6 DOF and it is then reduced to 2 and 3 DOFs. In chapter 3, a similar method based on the generation of orthogonal vectors as static deflections due to different load distributions is investigated for some FEM models. Moreover, the formulation of the static condensation as well as the exact dynamic condensation are presented. Chapter 3 also includes a comparison between the results obtained by the three methods.

Chapter 4 contains the application of the proposed method on the reduction of example structures, namely, a hybrid continuous discrete vehicle model and a coiled pipe

meshed in ANSYS. In this chapter, the eigenvalues are computed and the frequency response analyses are obtained.

Chapter 5 includes a proposed method to obtain the natural frequencies of arbitrary clamped plates with different shapes. This method is based on employing two dimensional boundary characteristic orthogonal polynomials in the Rayleigh-Ritz method. The resulting generalized mass and stiffness matrices are reduced using a set of independent vectors.

Chapter 6 includes the conclusions and the recommendation for future work.

Chapter 2

Employing orthogonal vectors of model reduction for discrete systems

The previous chapter briefly reviewed the Rayleigh-Ritz method and FEM, and provided a review of the literature on studies that used the BCOP technique for solution of continuous structures. Moreover, survey of earlier studies of discrete model reductions was presented. The generation of the boundary characteristic orthogonal vectors was described using two different methods: Gram-Schmidt and as done in [42]. In this chapter the model reduction is performed using Gram Schmidt orthogonalization to generate boundary characteristic orthogonal vectors. The method is applied to study a discrete model of a building.

Model reduction of discrete systems becomes necessary when the number of degrees of freedom is large and makes the analysis time consuming. The discrete systems can be separated into two categories. In the first category are the continuous systems which are discretized for analysis purpose such as FEM. In the second are those with springs, dampers and lumped masses. Purely discrete systems never occur in nature, and they are just a convenient way to model some problems. Between those two categories the reduction has been an important issue in the former, while at the same time it can be beneficial for some of the latter category if the number of degrees of freedom is quite

large. In this section, a high-rise building is modeled as a discrete system on which the model reduction is applied.

In the following, a set of orthogonal vectors is generated following Bhat [13] where Gram-Shmidt method is used to generate boundary characteristic orthogonal polynomials that are used as admissible functions in the Rayleigh-Ritz method for plate problems. Results are generated using the Langrage-Bhat approach where the orthogonal set is taken as a transformation to a set of generalized coordinates.

Many studies have showed that a valid building model should include the damping characteristic of the structure in order to study their response to earthquakes. In this example the damping is approximated as a set of inter-storey viscous dampers. Energy dissipation devices were studied by Soong and Dargush [46]. The optimum condition of a first storey viscous damper is investigated by Constantinou and Tadjbakhsh [47], while the result of distributing the viscoelastic dampers at different location in a shear building was studied by Hahn and Sathiavageeswaran [48]. An optimal design for framed structure was built by Lavan and Levy [49]. These studies, among others, have shown that base damping is less than all others and they concluded that increasing the base damping coefficient will result in better results in case of earthquakes.

2.1. Modeling

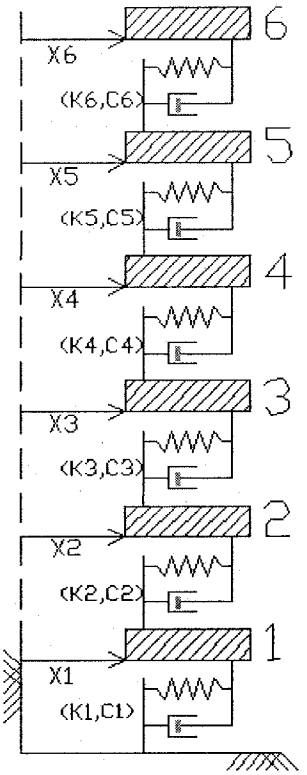

Fig. 2. Multi-storey building model.

The model of a six storey building is shown in Fig. 2. This building is assumed as a six degree of freedom system where each degree of freedom represents a floor. Precisely the first degree of freedom represents the basement and the rest are for other floors. The kinetic and potential energies and the damping functions are expressed, respectively, as

$$T = \frac{1}{2}\sum_{i=1}^{n} m_i \dot{x}_i^2$$

$$U = \frac{1}{2}\sum_{i=1}^{n} k_i (x_i - x_{i-1})^2 \qquad (1.1)$$

$$D = \frac{1}{2}\sum_{i=1}^{n} c_i (\dot{x}_i - \dot{x}_{i-1})^2$$

The base excitation is $x_b(t)$, which is assumed to be a harmonic excitation as follows:

$$x_b(t) = X_b \sin \omega t \qquad (1.2)$$

Eq. (1.1) and (1.2) can be rewritten in a matrix form as shown below:

$$T = \frac{1}{2}\{\dot{x}\}^T [M]\{\dot{x}\}$$

$$U = \frac{1}{2}(\{x - x_b\}^T [K]\{x - x_b\} \qquad (1.3)$$

$$D = \frac{1}{2}\{\dot{x} - \dot{x}_b\}^T [C]\{\dot{x} - \dot{x}_b\}$$

where $[M]$, $[K]$ and $[C]$ stand for the mass, stiffness and damping matrices, respectively, while $\{x\}$ and $\{x_b(t)\}$ are the displacement and base displacement vectors, respectively, shown below:

$$\{x\} = \{x_1, x_2, ...x_n\}^T \qquad (1.4)$$

$$\{x_b(t)\} = \{X_b, 0, 0, ..., 0\}^T \sin \omega t \qquad (1.5)$$

$[M]$, $[K]$ and $[C]$ matrices are shown in Eq. (1.6),(1.7) and (1.8), respectively, as

$$[M]=\begin{bmatrix} M_1 & 0 & 0 & 0 & 0 & 0 \\ 0 & M_2 & 0 & 0 & 0 & 0 \\ 0 & 0 & M_3 & 0 & 0 & 0 \\ 0 & 0 & 0 & M_4 & 0 & 0 \\ 0 & 0 & 0 & 0 & M_5 & 0 \\ 0 & 0 & 0 & 0 & 0 & M_6 \end{bmatrix} \tag{1.6}$$

$$[K]=\begin{bmatrix} K_1+K_2 & -K_2 & 0 & 0 & 0 & 0 \\ -K_2 & K_2+K_3 & -K_3 & 0 & 0 & 0 \\ 0 & -K_3 & K_3+K_4 & -K_4 & 0 & 0 \\ 0 & 0 & -K_4 & K_4+K_5 & -K_5 & 0 \\ 0 & 0 & 0 & -K_5 & K_5+K_6 & -K_6 \\ 0 & 0 & 0 & 0 & -K_6 & K_6 \end{bmatrix} \tag{1.7}$$

$$[C]=\begin{bmatrix} C_1+C_2 & -C_2 & 0 & 0 & 0 & 0 \\ -C_2 & C_2+C_3 & -C_3 & 0 & 0 & 0 \\ 0 & -C_3 & C_3+C_4 & -C_4 & 0 & 0 \\ 0 & 0 & -C_4 & C_4+C_5 & -C_5 & 0 \\ 0 & 0 & 0 & -C_5 & C_5+C_6 & -C_6 \\ 0 & 0 & 0 & 0 & -C_6 & C_6 \end{bmatrix} \tag{1.8}$$

2.2. Characteristic orthogonal vector set

In order to generate the set of characteristic orthogonal vectors, a procedure similar to that used by Bhat [10] is employed. This procedure demands the choice of a first

vector $\{\hat{\varphi}_1\}$ that is assumed as the static deflection due to a uniform load as an approximation to the first vibration mode. This vector is obtained as follows:

$$\{\hat{\varphi}_1\} = [K]^{-1}\{s\} \tag{1.9}$$

In Eq.(1.9) , $\{s\}$ stands for the uniform load.

$$\{s\} = [1,1,1,...,1]^T \tag{1.10}$$

At this stage Gram-Schmidt orthogonalization procedure is used to generate the rest of the vectors. Knowing that this method was originally used for continuous functions, some modifications are introduced to accommodate the discrete nature of the system.

The generation of the vectors is accomplished by the following set of equations:

$$\begin{aligned}
&\{\hat{\varphi}_2\} = ([y]-B_2)\{\hat{\varphi}_1\}, \quad \text{where} \\
&B_2 = \frac{\{\hat{\varphi}_1\}^T[M][y]\{\hat{\varphi}_1\}}{\{\hat{\varphi}_1\}^T[M]\{\hat{\varphi}_1\}}, \\
&\{\hat{\varphi}_{i+1}\} = ([y]-B_{i+1})\{\hat{\varphi}_i\} - C_{i+1}\{\hat{\varphi}_{i-1}\}, \quad \text{where} \\
&B_{i+1} = \frac{\{\hat{\varphi}_i\}^T[M][y]\{\hat{\varphi}_i\}}{\{\hat{\varphi}_i\}^T[M]\{\hat{\varphi}_i\}}, \qquad C_{i+1} = \frac{\{\hat{\varphi}_{i-1}\}^T[M][y]\{\hat{\varphi}_i\}}{\{\hat{\varphi}_{i-1}\}^T[M]\{\hat{\varphi}_{i-1}\}}
\end{aligned} \tag{1.11}$$

The matrix $[Y]$ is a matrix that represents the distance of each degree of freedom from the ground.

$$[Y]=\begin{bmatrix} 1 & 0 & 0 & 0 & 0 & 0 \\ 0 & 2 & 0 & 0 & 0 & 0 \\ 0 & 0 & 3 & 0 & 0 & 0 \\ . & & & . & & . \\ . & & & & . & . \\ . & . & . & . & . & n \end{bmatrix} \tag{1.12}$$

The orthogonalization is made using a weight function that is taken as the mass matrix. Assembling vectors $\{\hat{\varphi}\}$ results in a matrix $[\hat{\varphi}]$ whose columns are normalized as follows:

$$\{\varphi_i\}=\frac{\{\hat{\varphi}_i\}}{\left(\{\hat{\varphi}_i\}^T[M]\{\hat{\varphi}_i\}\right)^{\frac{1}{2}}},\ i=1,2,...,n \tag{1.13}$$

Concatenating the vectors $\{\varphi_i\}$ results in a matrix $[\varphi]$. This is used as transformation matrix to a set of generalized coordinate vector as follows:

$$\{x\}=[\varphi]\{q\} \tag{1.14}$$

Thus the energy expressions and the damping functions can be expressed in terms of the generalized coordinates following the Lagrange-Bhat approach [11].

$$\begin{aligned} T &= \frac{1}{2}([\varphi]\{\dot{q}\})^T[M]([\varphi]\{\dot{q}\}) \\ U &= \frac{1}{2}([\varphi]\{q\}-x_b)^T[K]([\varphi]\{q\}-x_b) \\ D &= \frac{1}{2}([\varphi]\{\dot{q}\}-\dot{x}_b)^T[C]([\varphi]\{\dot{q}\}-\dot{x}_b) \end{aligned} \tag{1.15}$$

The equation of motions in terms of generalized coordinates can be expressed as follows using Lagrange equations:

$$
\begin{aligned}
&[\mu]\{\ddot{q}\}+[\chi]\{\dot{q}\}+[\kappa]\{q\}=\{\sigma\},\\
&[\mu]=[\varphi]^T[M][\varphi],\quad [\kappa]=[\varphi]^T[K][\varphi],\\
&[\chi]=[\varphi]^T[C][\varphi],\ \{\sigma\}=[\varphi]^T K_1\{x_b\}+[\varphi]^T C_1\{\dot{x}_b\},
\end{aligned}
\tag{1.16}
$$

where K_1 and C_1 are the base stiffness and damping, respectively. Homogeneous form of Eq. (1.16) is solved for the eigenvalues and eigenvectors.

2.3. Results and discussion

The model shown in Fig.1 consists of 6 degrees of freedoms with the following structural data [50]: $M_1 = M_{base} = 6800\text{kg}$, $M_2 = M_3 = M_4 = M_5 = M_6 = 5879\,\text{kg}$ which are the mass of each floor. And the following are the values of the stiffness and damping:

$$
\begin{aligned}
&k_1 = 231.500\,kNm^{-1},\ k_2 = 33732\,kNm^{-1},\ k_3 = 29093\,kNm^{-1},\ k_4 = 28621\,kNm^{-1},\\
&k_5 = 24954\,kNm^{-1},\ k_6 = 19059\,kNm^{-1}\\
&c_1 = 7.480\,kNsm^{-1},\ c_2 = 67.000\,kNsm^{-1},\ c_3 = 56.000\,kNsm^{-1},\ c_4 = 57.000\,kNsm^{-1},\\
&c_5 = 50.000\,kNsm^{-1},\ c_6 = 38.000\,kNsm^{-1}
\end{aligned}
$$

The excitation amplitude X_b is taken as $0.01m$. The proposed orthogonal vectors are generated from Eq. (1.11) and plotted in Figs. 2-7. Those vectors represent the relative displacements of the degrees of freedom. As seen, all plots except Fig. 2 start from 0 which is the ground level where the displacement is always 0. However, the ground level is not shown in Fig. 2 due to the huge difference between the base displacement and

those of the floors. This is due to the lower base stiffness in comparison to that existing between the floors as shown in the structural data. Those plots show a resemblance with the mode shapes of a cantilever beam.

Fig. 3. Vector # 1 vs. floors.

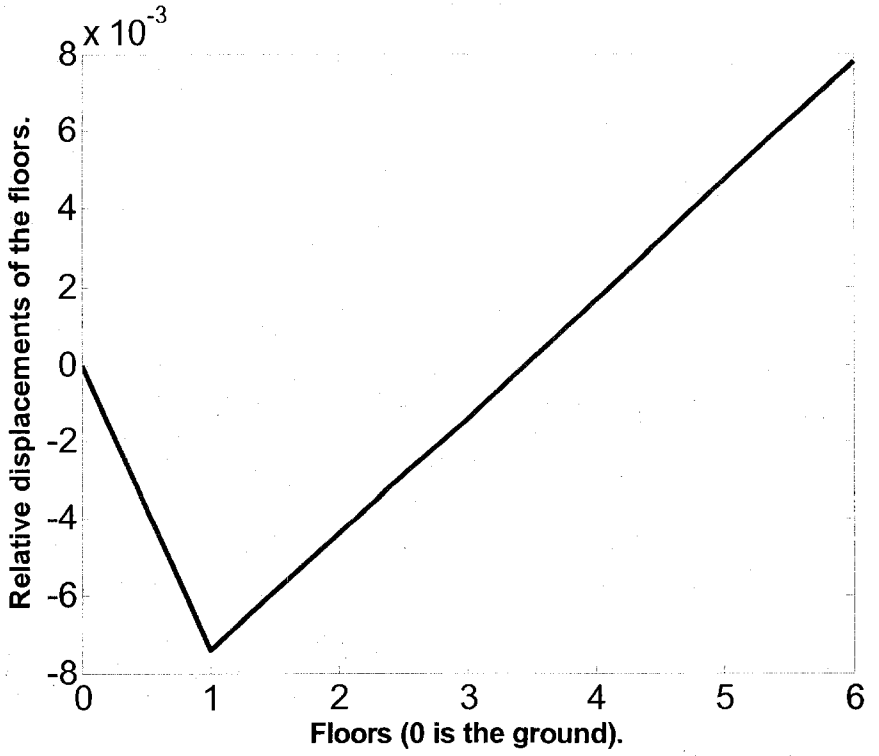

Fig. 4. Vector # 2 vs. floors.

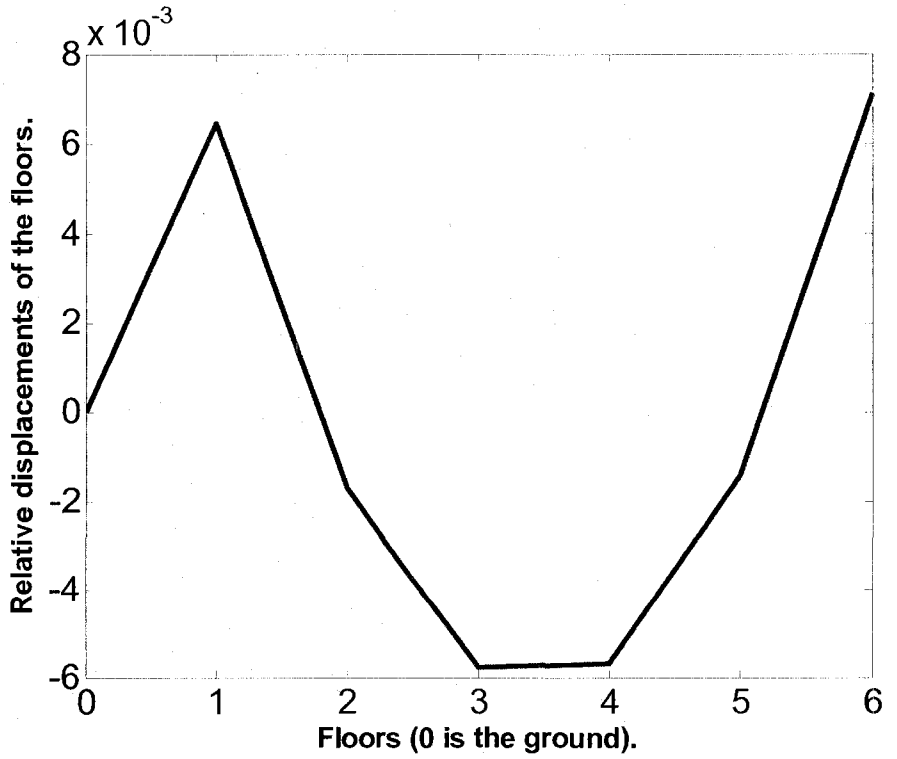

Fig. 5. Vector # 3 vs. floors.

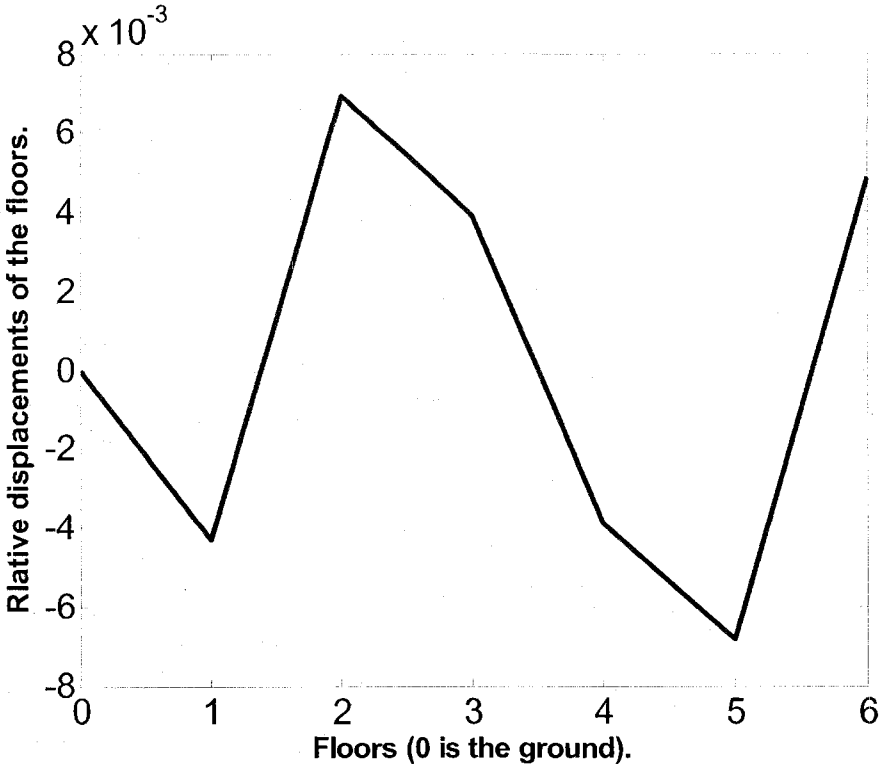

Fig. 6. Vector # 4 vs. floors.

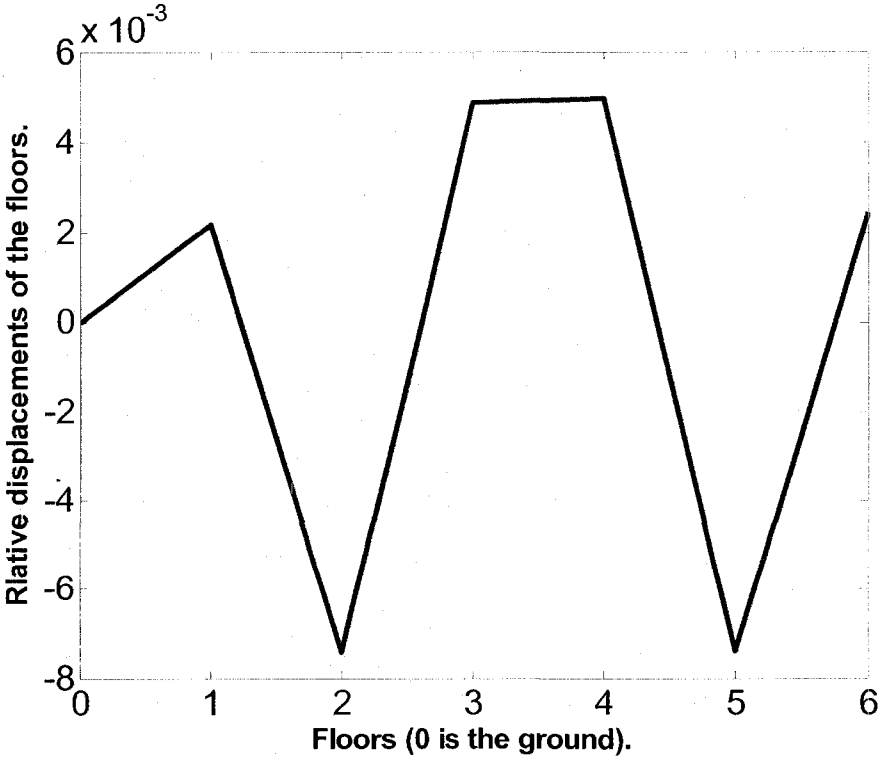

Fig. 7. Vector # 5 vs. floors.

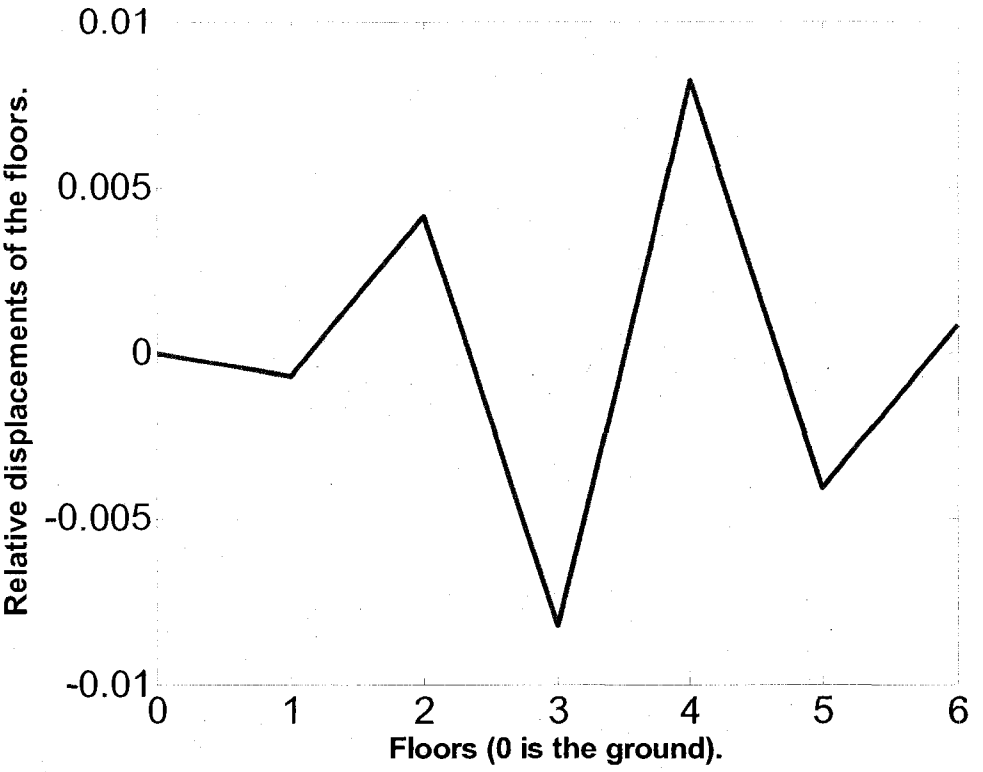

Fig. 8. Vector # 6 vs. floors.

Table 1. Natural frequencies of the structure.

Modes	Damped Natural Frequency (Hz.).	
	Exact	Approximated
First	0.3994	0.3994
Second	5.4608	5.4608
Third	10.271	10.271
Fourth	14.655	14.655
Fifth	18.2748	18.2748
Sixth	21.1266	21.1266

Table 1 shows the damped natural frequencies which are calculated from the complex eigenvalues of the system where the transformation matrix concatenates six vectors. As shown the values are the same which is expected since there is no reduction of the model order.

The transmissibility plots of the generalized coordinates (q) are shown in Fig. 8. This plot is obtained due to a harmonic base excitation of $0.01m$ amplitude. It shows a peak for the 1st generalized coordinate in the range of [0 0.5] Hz. Covering the 1st natural frequency. However, a smaller peak for the 2nd generalized coordinate in the range of [4.9 5.7] Hz. which covers the 2nd natural frequency, is present. This may be caused by the small coupling in $[\mu]$, $[\chi]$ and $[\kappa]$. Note that if the modal matrix was to be considered as the transformation matrix $[\varphi]$, the resulting transformed matrices $[\mu]$, $[\chi]$ and $[\kappa]$ would have been diagonal without any coupling. It should be noted that smaller peaks will show for different generalized coordinates for the rest of the natural frequencies, however these peaks are small enough to be neglected.

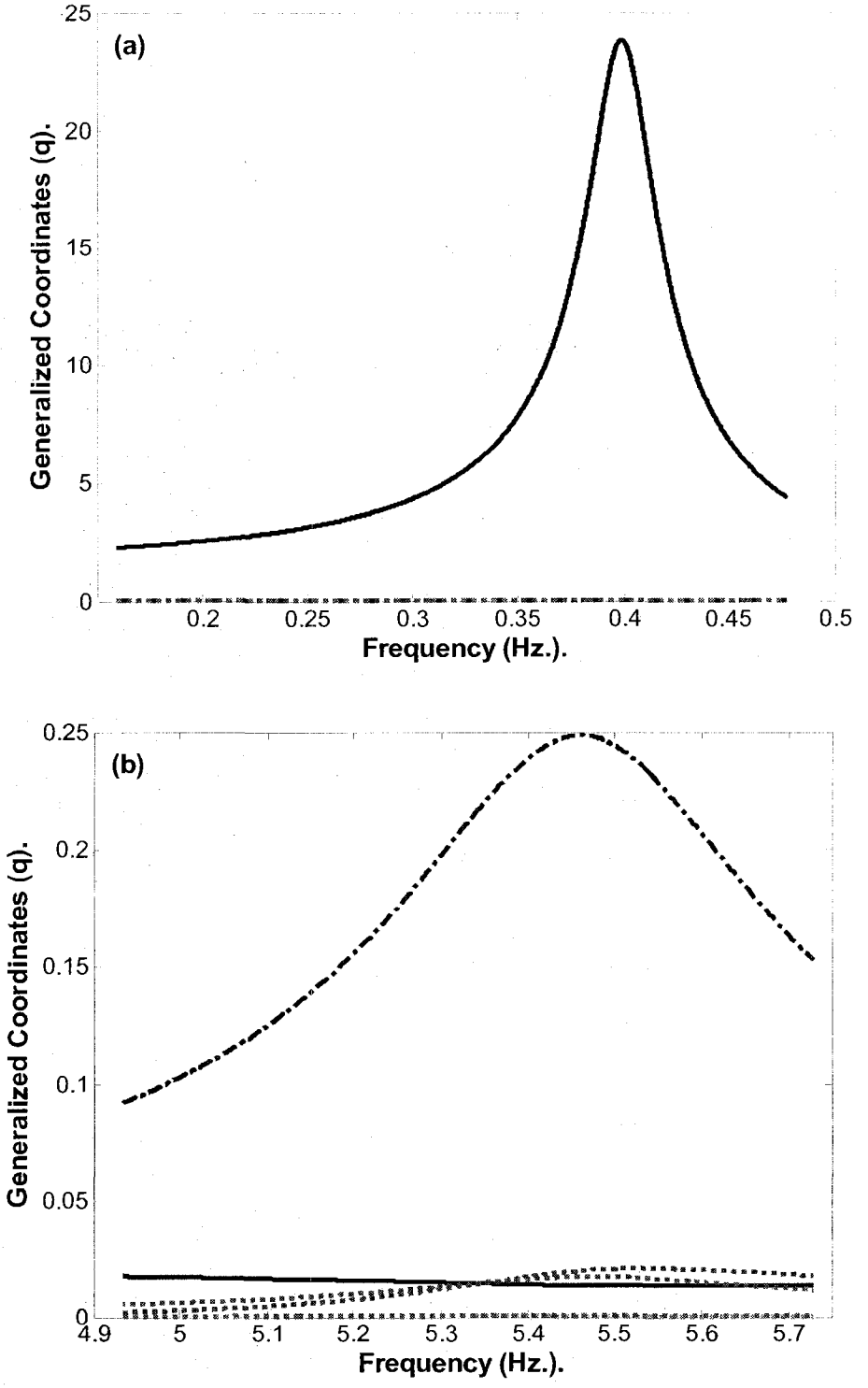

Fig. 9.Transmissibility plots of the generalized coordinates. (a) Frequency range [0, 0.5]. (b) Frequency range [4.9, 5.75]. _____ 1st Generalized coordinate, .-.-.-.- 2nd generalized coordinate, - - - - - - - 3rd, 4th, 5th and 6th generalized coordinates.

2.4. Dynamic reduction

In this section the reduction is applied on the discrete system with the six degree of freedom system. Two cases are considered, first reduction is from 6 to 2 and the second is from 6 to 3. The error is computed and compared to the exact value of the complete model. The error in computing the natural frequencies is dependent on the number of vectors employed for thc reduction. For example if 2 vectors are used to reduce the system, the error at the second one will be significantly large compared to the case where 3 vectors are used.

Table 2. Reduced model natural frequencies.

Modes.	Damped Natural Frequency (Hz.).		Error. (%)
	Exact	Approximated	
1.First	0.3994	0.3994	0
2.Second	5.4608	5.6301	3.1

Table 3. Reduced model natural frequencies.

Modes.	Damped Natural Frequency (Hz.).		Error. (%)
	Exact	Approximated	
1.First	0.3994	0.3994	0
2.Second	5.4608	5.5466	1.57
3.Third	10.271	10.7948	5.1

The reduced damped natural frequencies and the corresponding error in comparison with the exact ones are shown in Tables 2 and 3. As mentioned earlier, the error in the second natural frequency is less when three vectors are employed instead of two. Generalizing this fact, it can be said that when a better approximation of the third value is desired a higher number of vectors should be used.

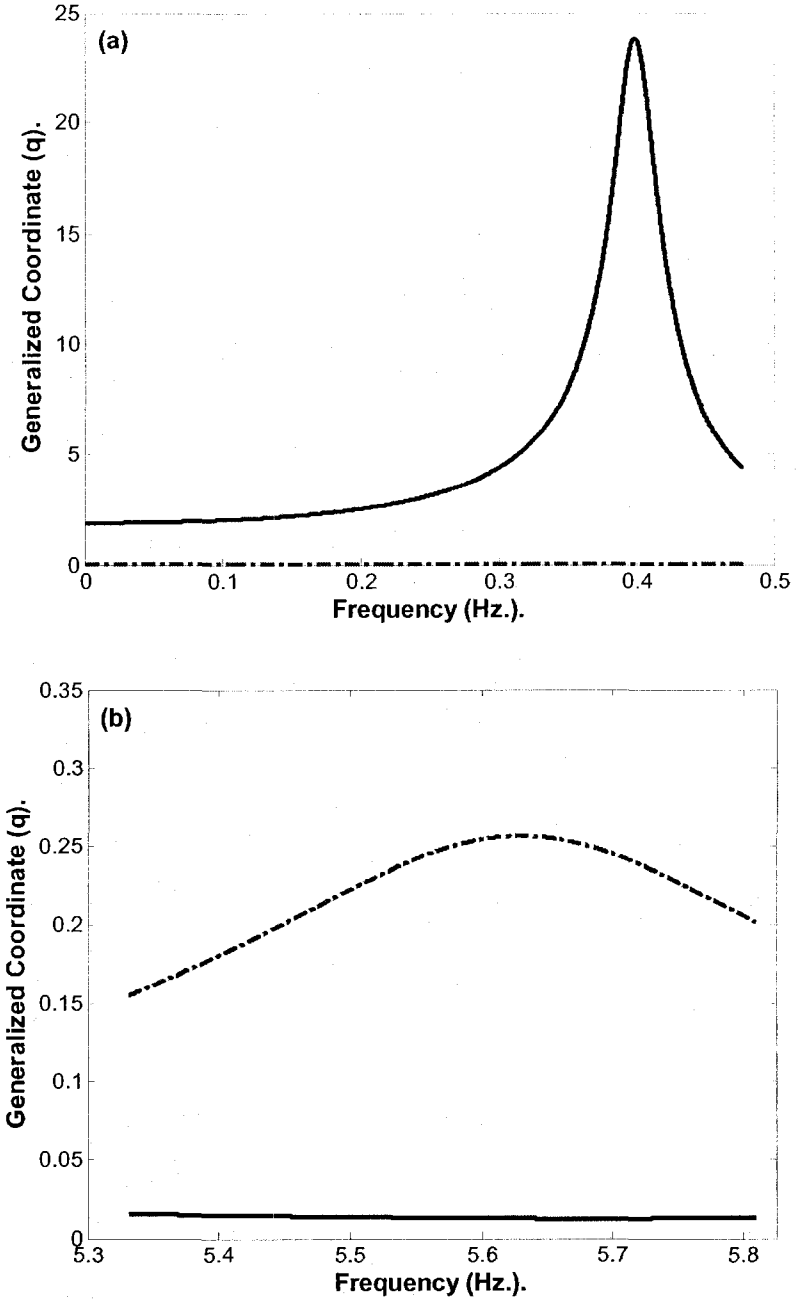

Fig. 10. Transmissibility plots of first and second generalized coordinates of the reduced model. (a) Frequency range [0, 0.5]. (b) Frequency range [5.25, 5.75]. _____ 1st Generalized coordinate, _ _ _ _ _ 2nd generalized coordinate.

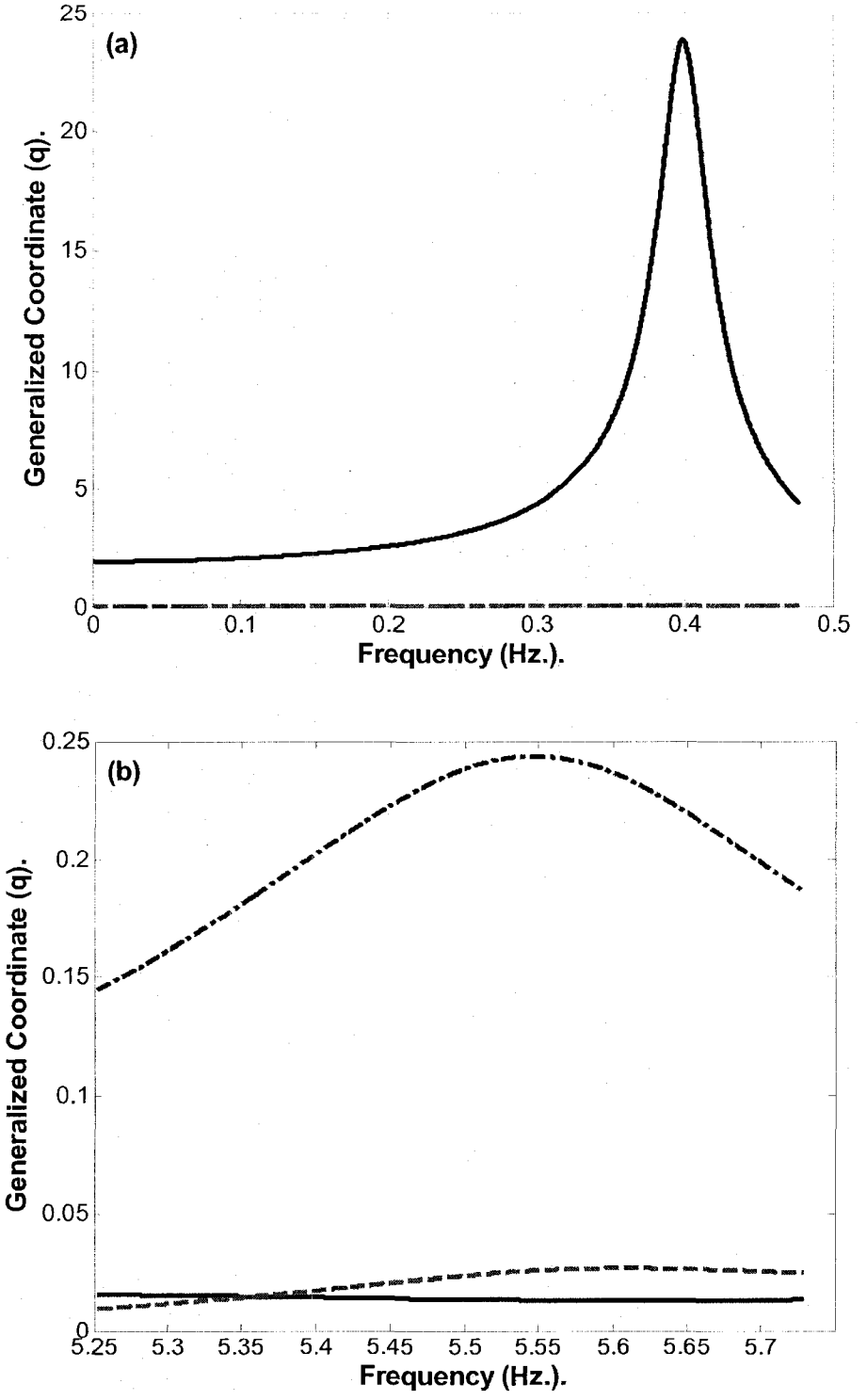

Fig. 11. Transmissibility plots of the first, second and third generalized coordinates of the reduced model. (a) Frequency range [0, 0.5]. (b) Frequency range [5.25, 5.75]. _____ 1st Generalized coordinate, - - - - - - 2nd generalized coordinate, _ _ _ _ _ _ _ 3rd generalized coordinate.

Fig.9 and Fig.10 show the transmissibility plots of the reduced systems generalized coordinates for $0.01m$ amplitude excitation, where two and three vectors were used, respectively. Those plots are obtained for frequency ranges covering the two first natural frequencies in both cases. The peak in Fig.9(b) occurs at 5.63 Hz. similarly to that calculated and showed in Table 2. Similarly Fig.10(b) shows the peak at 5.54 Hz. which is seen in Table 3.

The next chapter will discuss the model reduction of FEM models using boundary characteristic orthogonal vectors.

Chapter 3

Employing orthogonal vectors for model reduction of FEM models.

The reduction was applied to a building model using a set of characteristic orthogonal vectors generated using Gram-Schmidt method in the last chapter. In the current chapter the method is extended to FEM models.

Model reduction of Finite Element models is of particular interest in view of the large number of degrees of freedom in modeling real structures. Large number of degrees of freedom is necessary in FEM modeling in order to obtain satisfactory results.

Model reductions in FEM were carried out in different ways such as substructuring, condensation and eigenvalue economization. An excellent review of the major approaches is presented by Leung [45]. In the present chapter a review of the two major techniques is presented and a new method is proposed. Among the earlier studies the exact dynamic condensation and the static condensation or eigenvalue economization are frequently used and are briefly described here.

3.1. Exact dynamic condensation.

A Finite Element analysis for structural vibration will yield a system of ordinary differential equations. This system results in an eigenvalue problem.

$$[D]\{x\}=\{F\} \tag{3.1}$$

where $[D]$ is the dynamic stiffness matrix and is obtained by the assumption of a harmonic motion in time and separation of variables. The vectors $\{x\}$ and $\{F\}$ are the displacement vectors and the applied forces or moments, respectively.

$$[D]=[K]-\omega^2[M] \tag{3.2}$$

In the conventional method the slave and master degrees of freedom are chosen such that the slaves are those that are not driven by any forces. Thus equation (3.1) can be rewritten as follows:

$$\begin{bmatrix} D_{mm} & D_{ms} \\ D_{sm} & D_{ss} \end{bmatrix} \begin{Bmatrix} x_m \\ x_s \end{Bmatrix} = \begin{Bmatrix} F \\ 0 \end{Bmatrix} \tag{3.3}$$

in which m and s stand for master and slave DOFs, respectively. This system of equations can be separated into two parts as follows:

$$\begin{aligned} [D_{mm} \quad D_{ms}] \begin{Bmatrix} x_m \\ x_s \end{Bmatrix} &= \{F\} \\ [D_{sm} \quad D_{ss}] \begin{Bmatrix} x_m \\ x_s \end{Bmatrix} &= \{0\} \end{aligned} \tag{3.4}$$

In order to eliminate the slave DOFs, $\{x_s\}$ is written in terms of $\{x_m\}$, using the second part of Equation (3.4), as follows:

$$\{x_s\} = -[D_{ss}]^{-1}[D_{sm}]\{x_m\} \tag{3.5}$$

Substituting this $\{x_s\}$ in the first part of Equation (3.4) , the system of equations can be written as follows:

$$\left[[D_{mm}]-[D_{ms}][D_{ss}]^{-1}[D_{sm}]\right]\{x_m\}=\{F\} \tag{3.6}$$

Let $\left[D^*\right]=[D_{mm}]-[D_{ms}][D_{ss}]^{-1}[D_{sm}]$, for simplification, and equation (3.6) becomes:

$$[D]^*\{x_m\}=\{F\} \tag{3.7}$$

Richards and Leung [51] proved that the mass matrix is equal to the derivative of the dynamic matrix with respect to ω^2, which can be seen from Equation (3.2). Consequently,

$$[M]=-\frac{\partial}{\partial(\omega^2)}[D] \tag{3.8}$$

Differentiating $\left[D^*\right]$ with respect to ω^2 will yield the condensed mass matrix as:

$$\begin{aligned}\left[M^*\right]=[M_{mm}]-[D_{ms}][D_{ss}]^{-1}[M_{sm}]-[M_{ms}][D_{ss}]^{-1}[D_{sm}]\\ +[D_{ms}][D_{ss}]^{-1}[M_{ss}][D_{ss}]^{-1}[D_{sm}]\end{aligned} \tag{3.9}$$

where $\frac{\partial}{\partial\omega^2}[D]^{-1}$ is obtained by differentiating the identity, $[D]^{-1}[D]=[I]$.The reduced stiffness matrix can be then obtained using the following relation:

$$\left[K^*\right]=\left[D^*\right]+\omega^2\left[M^*\right] \tag{3.10}$$

The reduced eigenvalue problem is then shown as follows:

$$\left[K^*\right]-\omega^2\left[M^*\right]=\{F\} \tag{3.11}$$

This method requires the inverse of the dynamic matrix during the computation of the natural frequencies.

3.2. Static condensation

The static condensation was first proposed by Guyan [30] and Irons [31]. This method was later known as Guyan reduction or eigenvalue economization. The main idea in this method is to eliminate the slave degrees of freedom in terms of the master DOFs. This choice is mainly related to the distribution of energy. Thus for different modes different selection of master and slave DOFs is required.

Similar to the exact dynamic condensation, the reduced eigenvalue problem will have the same form as in Eq. (3.6). However, in this method a major assumption is used by taking the inverse of $\left[D_{ss}\right]$ in Eq. (3.6) as follows:

$$\left[D_{ss}\right]^{-1}=\left[K_{ss}\right]^{-1}-\omega^2\left[K_{ss}\right]^{-1}\left[M_{ss}\right]\left[K_{ss}\right]^{-1} \tag{3.12}$$

3.3. Boundary characteristic orthogonal vectors in the Rayleigh-Ritz analysis

The Rayleigh-Ritz method was originally introduced as an extension of Rayleigh's method and they were mainly used for continuous structures. However this method can

be applied to discrete systems also. Thus any discrete system can be reduced to a lower number of degrees of freedom.

A more general method than that used in chapter 1 is followed to generate a set of orthogonal vectors using the stiffness and mass matrices that satisfy all the requirements of the flexibility as well as the boundary conditions of the structure under study, using a procedure that was first introduced by Leger, Wilson and Clough [42].

3.3.1. Modified Gram-Schmidt method

The method of generating orthogonal vectors using Gram-Schmidt orthogonalization is modified here based on the fact that some DOF may be dependent. The mass and stiffness matrices can be rearranged to separate the slope from the deflection degrees of freedom. The mass and stiffness matrices can be rewritten as follows:

$$[M]=\begin{bmatrix}[M_{dd}] & [M_{ds}]\\ [M_{sd}] & [M_{ss}]\end{bmatrix} \quad [K]=\begin{bmatrix}[K_{dd}] & [K_{ds}]\\ [K_{sd}] & [K_{ss}]\end{bmatrix} \tag{3.13}$$

where the subscript "s" is for slopes and "d" is for deflections. As before, starting from a uniform load the first vector is computed as the static deflection as shown in Eq. (1.9) . Any other vector in the orthogonal vector set can be written as follows:

$$\varphi_i = \begin{Bmatrix}\varphi_{d,i}\\ \varphi_{s,i}\end{Bmatrix} \tag{3.14}$$

Using Gram-Schmidt orthogonalization the second and the rest of the vectors are obtained in the following two equations, respectively.

$$\varphi_2 = x\varphi_1 - b_2\varphi_1 \tag{3.15}$$

$$\varphi_{i+2} = x\varphi_{i+1} - b_{i+2}\varphi_{i+1} - c_{i+2}\varphi_i \tag{3.16}$$

Taking only the deflection into account in Eq. (3.15) yields the deflection portion of the second vector as:

$$\varphi_{d,2} = x\varphi_{d,1} - b_2\varphi_{d,1} \tag{3.17}$$

Since the slopes are the derivatives of the deflections, we have

$$\varphi_{s,2} = \frac{\partial\left(\varphi_{d,2}\right)}{\partial x} = \varphi_{d,1} + x\varphi_{s,1} - b_2\varphi_{s,1} \tag{3.18}$$

Combining the slopes and deflections the vector φ_2 can be written as follows:

$$\varphi_2 = \begin{Bmatrix} \varphi_{d,2} \\ \varphi_{s,2} \end{Bmatrix} = x\begin{Bmatrix} \varphi_{d,1} \\ \varphi_{s,1} \end{Bmatrix} - b_2\begin{Bmatrix} \varphi_{d,1} \\ \varphi_{s,1} \end{Bmatrix} + \begin{Bmatrix} 0 \\ \varphi_{d,1} \end{Bmatrix} \tag{3.19}$$

Proceeding similarly, the higher members of the orthogonal set are obtained as

$$\varphi_{i+2} = \begin{Bmatrix} \varphi_{d,i+2} \\ \varphi_{s,i+2} \end{Bmatrix} = x\begin{Bmatrix} \varphi_{d,i+1} \\ \varphi_{s,i+1} \end{Bmatrix} - b_{i+2}\begin{Bmatrix} \varphi_{d,i+1} \\ \varphi_{s,i+1} \end{Bmatrix} - c_{i+2}\begin{Bmatrix} \varphi_{d,i} \\ \varphi_{s,i} \end{Bmatrix} + \begin{Bmatrix} 0 \\ \varphi_{d,i+1} \end{Bmatrix} \tag{3.20}$$

These modifications will help in getting a better admissible vector in the Rayleigh-analysis resulting in a better convergence to the exact eigenvalues. However, this method becomes quite complicated in case of complex structures.

3.3.2. Boundary characteristic orthogonal vectors by static deflection

In this method the calculation of static deflections due to a load distribution that is proportional to the previous deflection vector is used. This method is also sensitive to the first vector assumption. Knowing that the static deflection corresponds to zero frequency, it is taken as the first eigenvector or mode shape which is the closest to zero. The static deflections automatically satisfy the geometrical boundary conditions.

As before, starting from a vector similar to that of Eq. (1.9) the rest of the vectors are obtained using the algorithm shown in Fig.12 and 13. This algorithm consists of three major computational steps:

- Computing the static deflection.
- Subtracting the contribution of the previous vectors for orthogonalization.
- Normalization.

Fig.12 and Fig.13 basically show the same information, however, in the later the algorithm is shown in a block diagram highlighting the two loops. It should also be noted that the stiffness matrix is a constant matrix and hence needs to be inverted once and stored for use when needed. This step is shown also in Fig.13 where the inverse of the stiffness matrix is stored as $[A]=[K]^{-1}$.

1. $\{y_1\}^T = [K]^{-1}\{s\}$ where $\{s\} = \{1 \quad 1 \quad 1 \quad \ldots \quad 1\}^T$

$$\{\phi_1\} = \frac{\{y_1\}}{\left(\{y_1\}^T [M]\{y_1\}\right)^{\frac{1}{2}}}$$

2. Higher member $\{\phi_i\}$ (i=2,3,4,…,n=number of desired vector):

- $\{y_i\} = [K]^{-1}[M]\{\phi_{i-1}\}$
- Orthogonalization (j=1,2,3,…,i-1)

$$a_{ij} = \phi_j^T [M]\{y_i\}$$

$$\{\hat{\phi}_i\} = \{y_i\} - \sum_{j=1}^{i-1} a_{ij}\{\phi_j\}$$

$$\{y_i\} = \{\hat{\phi}_i\}$$

- Normalization:

$$\{\phi_i\} = \frac{\{\hat{\phi}_i\}}{\left(\{\hat{\phi}_i\}^T [M]\{\hat{\phi}_i\}\right)}$$

Fig.12: Algorithm for the generation of orthogonal vectors.

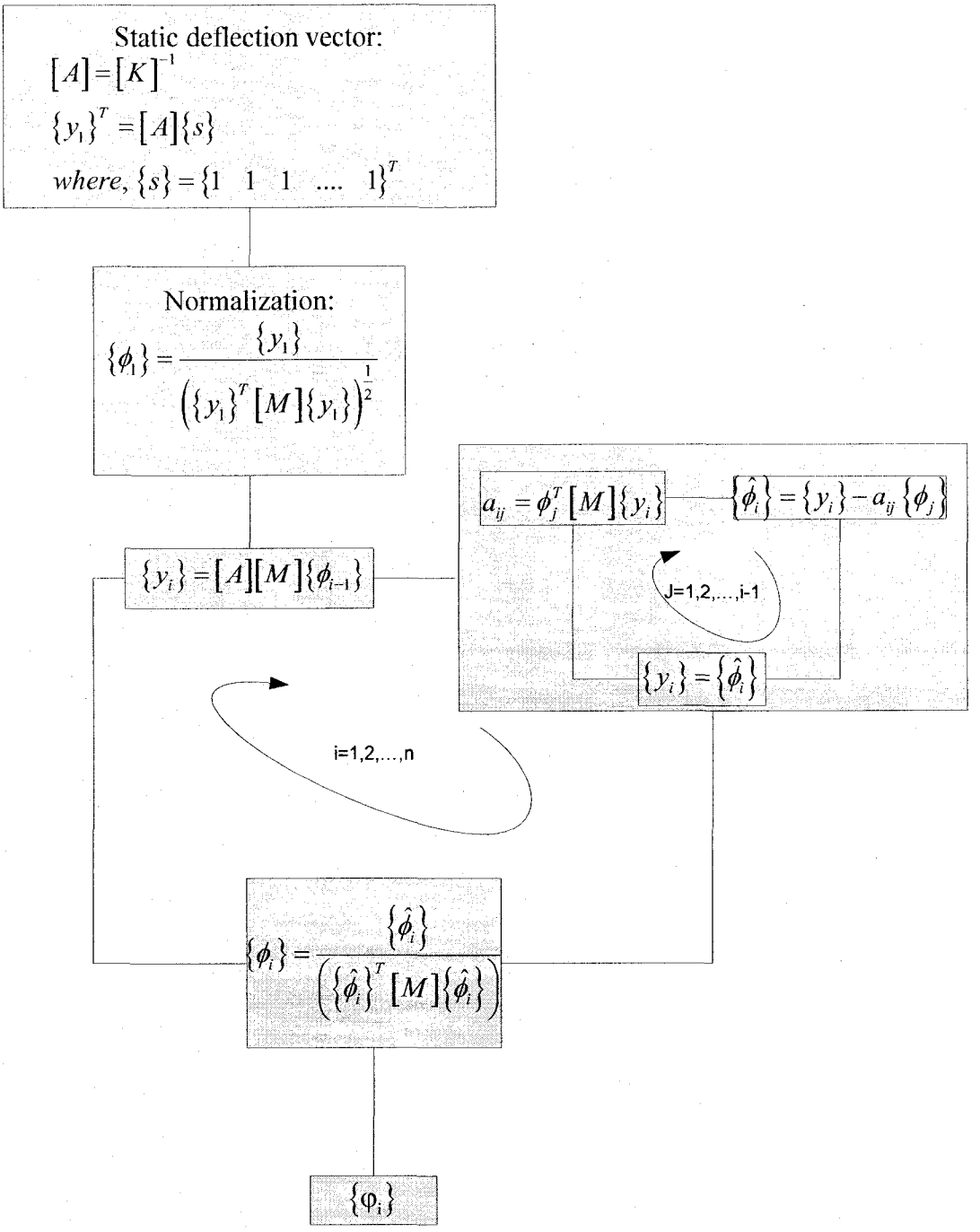

Fig.13: Computation scheme for the generation of orthogonal vectors.

3.4. Comparison of different model reduction techniques

A close examination of both the static and the exact dynamic condensations will easily show that both methods use a transformation from the complete model to the reduced one. This transformation can easily be described in terms of the rearranged matrices using slave and master DOFs. However, when both Gram-Schmidt method and the algorithm in Fig.13 are used the transformation lacks an explicit form in terms of the given matrices. It should also be noted that extending the condensation methods for substructuring may be difficult in some application due to the problem of matrix multiplication size.

Table 4: Transformation formulae for different methods.

Method	Transformation formulae:
Static condensation	$\begin{Bmatrix} x_m \\ x_s \end{Bmatrix} = \begin{bmatrix} [I] \\ [-K_{ss}^{-1}][K_{sm}] \end{bmatrix} \{x_m\}$
Exact dynamic condensation	$\begin{Bmatrix} x_m \\ x_s \end{Bmatrix} = \begin{bmatrix} [I] \\ -[D_{ss}]^{-1}[D_{sm}] \end{bmatrix} \{x_m\}$
Orthogonal vectors in Rayleigh-Ritz	$\{x\} = [\Phi]\{q\}$

$[\Phi]$ is the matrix of orthogonal vectors

Using this method of formulation, the computation of the reduced order model becomes very simple and it shows that all the listed methods are basically similar. The general form of the reduced order model matrices can be written as the following matrix product where $[T_r]$ stands for the transformation matrix:

$$[\kappa]=[T_r]^T[K][T_r] \qquad [\mu]=[T_r]^T[M][T_r] \tag{3.21}$$

3.5. Example structures

A set of example structures were investigated in order to compare different model reduction methods. Both methods that use a set of orthogonal vectors are compared together and the one using static deflection vectors is compared with both static and exact dynamic condensations.

3.5.1. Cantilever beam

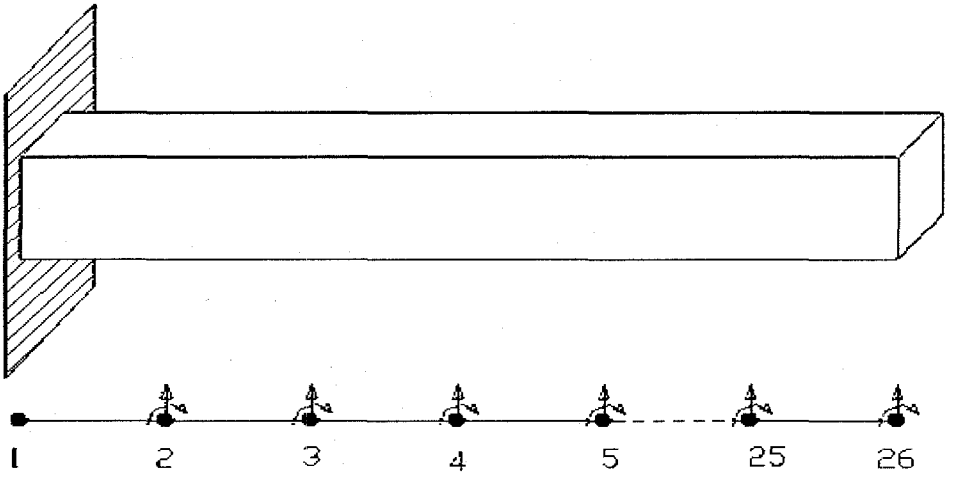

Fig. 14: Model of a cantilever beam.

A steel cantilever beam meshed into finite elements using one-dimensional beam elements is investigated. The current section includes the results for all the listed methods with different trials using different choices of master and slave DOFs. Eigenvalues are computed and the mode shapes are plotted. The current model shown in Fig. 14 is

meshed into 25 elements resulting in 26 nodes and 50 DOFs since two DOFs are constrained at the first node.

Table 5 shows the comparison of the reduced eigenvalues from both methods using orthogonal vectors in the Rayleigh-Ritz method. The comparison shows that the modified Gram-Schmidt method was capable to deal with the dependant DOFs resulting from the slope degrees of freedom in the FEM model. Both methods have given good results for up to half of the reduced order model, however, the second method has a better accuracy and also gives a better approximation to the higher modes.

Table 5: Comparison between exact and reduced eigenvalues of both Modified Gram-Schmidt and Static load in the Rayleigh-Ritz method.

Modes	Modified Gram-Schmidt		Static deflections in the Rayleigh-Ritz.		Exact
	values	Error (%)	value	Error (%)	
1	41.7801	0.0103	41.7758	0	41.7758
2	261.8121	0.0027	261.8049	0	261.8049
3	733.0768	0.0015	733.0655	0	733.0655
4	1436.571	0.002	1436.5432	0	1436.5432
5	2375.352	0.0227	2374.8139	0	2374.8139
6	3595.301	1.3371	3547.8678	0	3547.8632
7	5123.112	3.3719	4959.5926	0.0725	4956.0014
8	9040.585	36.9841	6791.0651	2.8991	6599.733
9	12773.29	50.6313	11007.8886	29.8124	8479.8412
10	59986.31	466.044	77951.9551	635.571	10597.4653

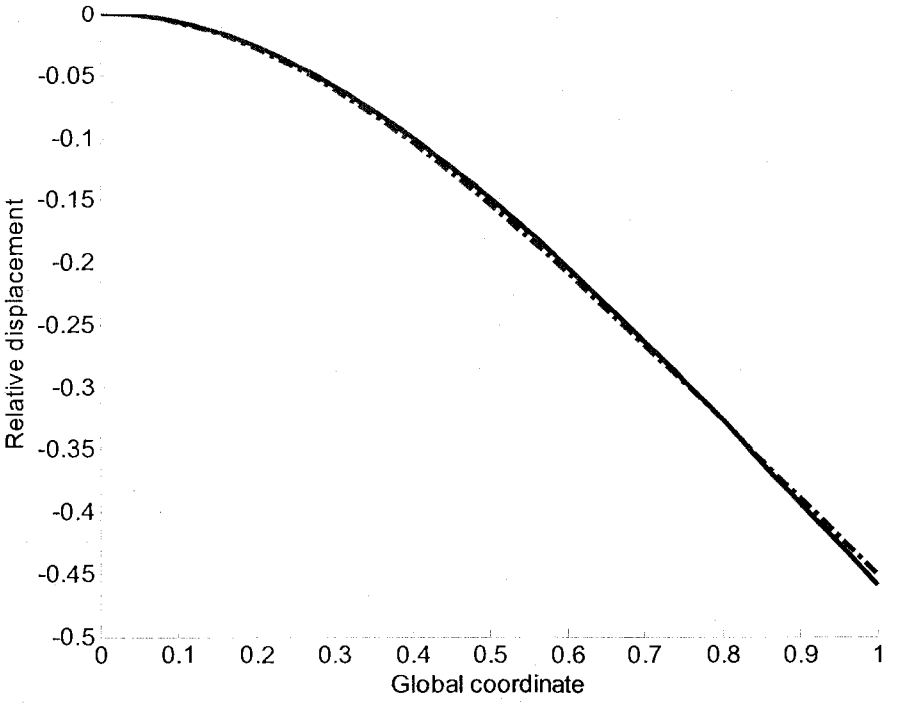

Fig. 15. Comparison of the first mode with assumed vectors. _____ Exact mode, - - - - - - - modified Gram-Schmidt, ... static deflection vectors.

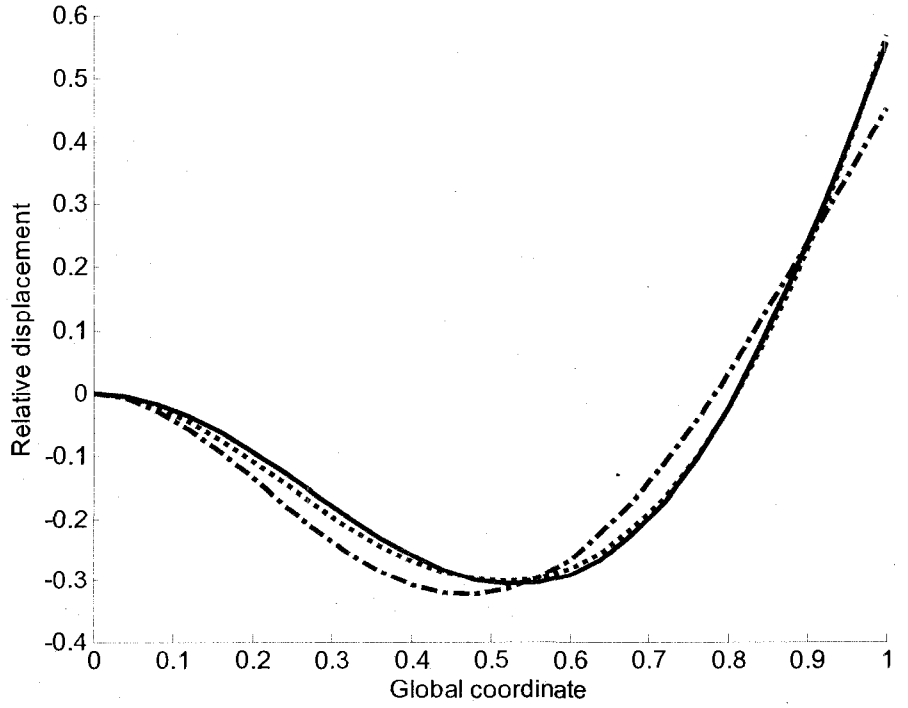

Fig. 16. Comparison of the second mode with assumed vectors. _____ Exact mode, - - - - - - - modified Gram-Schmidt, ... static deflection vectors.

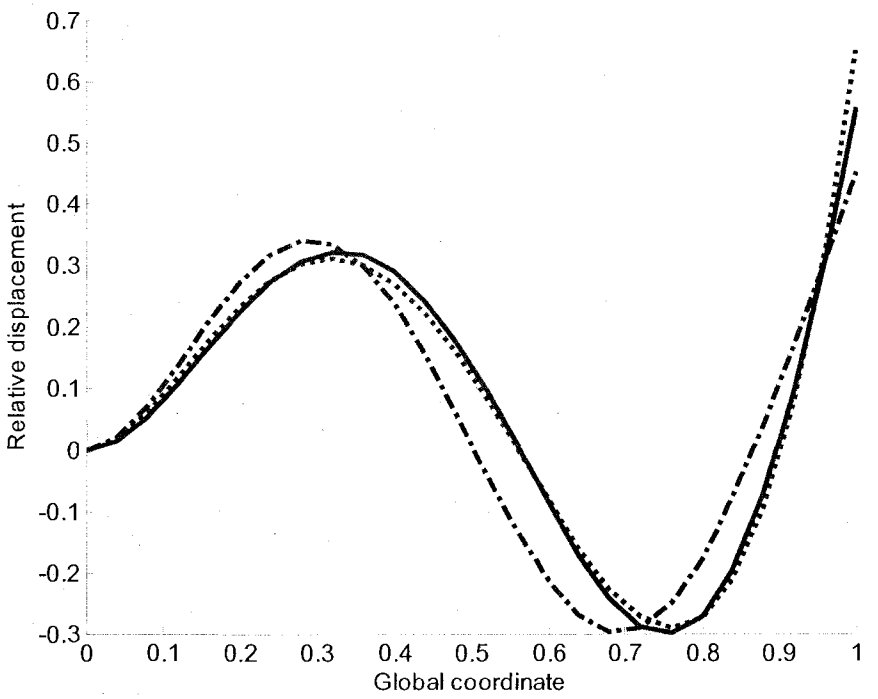

Fig. 17. Comparison of the third mode with assumed vectors. _____ Exact mode, _ _ _ _ _ _ _ modified Gram-Schmidt, _._._._.static deflection vectors.

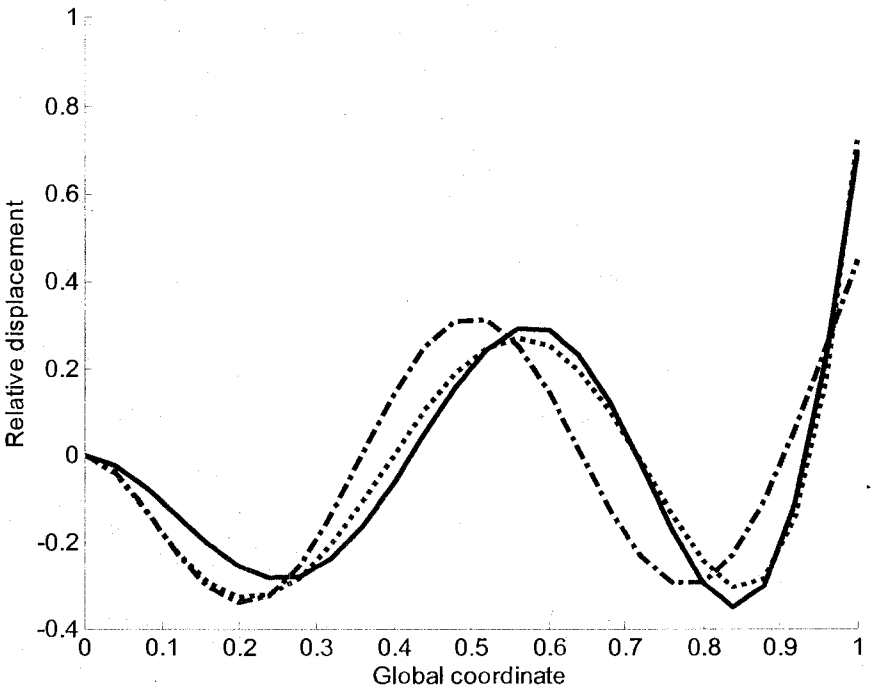

Fig. 18. Comparison of the fourth mode with assumed vectors. _____ Exact mode, _ _ _ _ _ _ _ modified Gram-Schmidt, _._._._.static deflection vectors.

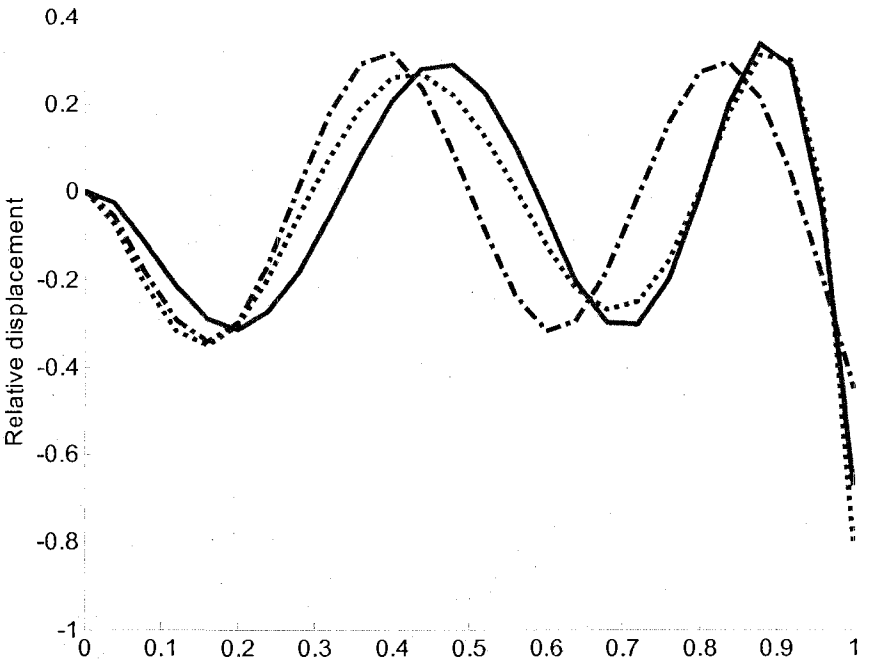

Fig.19. Comparison of the fifth mode with assumed vectors. _____ Exact mode, _._._._static deflection vectors, _ _ _ _ _ _ _ modified Gram-Schmidt.

Fig. 15 to 19 show the comparison between the exact eigenvectors calculated from FEM and the assumed vectors from both methods. The results show that the vectors resulting from modified Gram-Schmidt method are closer to the exact vectors than that of the deflection due to static load. However, the eigenvalues of the latter are closer to the exact ones than the former. This can be justified by the fact that the static deflection vectors satisfy the flexibility restriction of the system since the inverse of the stiffness matrix is used to calculate all the vectors which will ensure that the vectors satisfy all the boundary conditions. It should be noted that the plots of the vectors are based on the deflection only.

The same cantilever beam is also reduced using static and dynamic condensation methods. Different choices of the master degrees of freedom are taken and for every case the results are presented and discussed. First, the master DOFs are chosen to be on node 22 to 26 of the model shown in Fig. 14. This resulted in a reduction to a (10×10) reduced order model. Further, the model was reduced by the choice of different master DOF where they have been chosen along the span of the beam, namely, nodes 1, 4, 9, 13... 49.

Table 6 shows a comparison between the reduced order model natural frequencies using the three different methods. It should be noted that the selection of the master DOF has resulted in the loss of some modes. The numbers in parenthesis gives the equivalent mode of the complete structure. As shown, the exact dynamic condensation will give always very close results, however, this method is an iterative method that needs to converge toward the exact solution at each frequency of interest. Hence it makes the process computationally demanding. Moreover it is affected by the choice of the master DOFs. The static condensation method shows good results at the first frequency which is closer to 0 or the static condition. The use of orthogonal vectors in the Rayleigh-Ritz method gives good results without the need to choose either the master or slave DOFs. This method will also guarantee the sequence of modes, in other words the resulting reduced modes will always be in an ascending sequence due to the nature of this method that applies the Rayleigh-Ritz analysis. Moreover, the error in the higher modes can easily be reduced by using a larger number of vectors if desired.

Table 6: Comparison between the reduced eigenvalues of different reduction methods.

Mode	Dynamic condensation.		Static condensation.		Static load vectors in Rayleigh-Ritz.	
	Values (Hz.)	Error (%)	Value (Hz.)	Error (%)	Values (Hz.)	Error (%)
1	41.7758	(1) 0	41.8224	(1) 0.11	41.7758	0
2	261.8049	(2) 0	315.3932	(2) 20.4688	261.804	0
3	6599.733	(8) 0	2896.8566	295.170	733.065	0
4	32278.326	(17) 0	12255.104	753.0968	1436.54	0
5	66693.639	(24) 0	30907.010	1201.4498	2374.81	0
6	113667.0506	(30) 0	58863.057	1559.1129	3547.86	0
7	165892.2678	(35) 0	107700.19	2073.1268	4959.59	0.0725
8	236813.1874	(40) 0	171984.56	2505.9322	6791.06	2.8991
9	322578.9028	(45) 0	271107.71	3097.0848	11007.8	29.8124
10	444651.1542	(50) 0	442445.70	4075.0144	77951.9	635.571

Table **7** shows the natural frequencies of the cantilever beam using a reduced model and with a better choice of master DOF. It is clearly shown that the natural frequencies, calculated from dynamic condensation, show a better result always with negligible error. However, the static condensation gives poor results. This is because this method searches for the static deflection state at which the beam has its maximum energy located at the master DOFs.

Table 7: Comparison between the reduced eigenvalues of different reduction methods.

Mode	Dynamic condensation.		Static condensation.		Static load vectors in Rayleigh-Ritz.	
	Values (Hz.)	Error (%)	Value (Hz.)	Error (%)	Values (Hz.)	Error (%)
1	41.7758	(1) 0	2508.3685	(5) 5.6238	41.7758	0
2	261.8049	(2) 0	6359.0402	(8) 3.6470	261.804	0
3	733.0655	(3) 0	7739.6378	(9) 8.7290	733.065	0
4	1436.5432	(4) 0	9349.6256	----------	1436.54	0
5	2374.8139	(5) 0	13754.140	(11) 6.1753	2374.81	0
6	3547.8632	(6) 0	16327.307	(12) 4.9846	3547.86	0
7	4956.0014	(7) 0	20640.528	(14) 3.9215	4959.59	0.0725
8	6599.733	(8) 0	22496.269	(14) 4.7167	6791.06	2.8991
9	8479.8412	(9) 0	24703.337	(15) 0.4837	11007.8	29.8124
10	55673.9094	(22) 0	31415.925	(17) 2.6718	77951.9	635.571

3.5.2. Simply supported beam

The case of a simply supported beam is studied using both the dynamic condensation and the orthogonal vectors in the Rayleigh-Ritz method. The results, shown in Table 8, highlight the sensitivity of the dynamic condensation on the correct choice of the master degrees of freedom. In this case also the same number as well as the same choice of degrees of freedom as in the second case in the cantilever beam have been used. This choice gave good results in the case of cantilever beams, however, it was not capable to do so in the case of simply supported beams.

Moreover, the error in the sixth natural frequency using the orthogonal vectors came to be higher than that of the fifth. This should not happen usually in the Rayleigh-Ritz method, however, this might have been due to some poorly scaled vector, which includes very large numbers compared to the others. A very good study about the effect of

assumed mode components on the results of Rayleigh-Ritz analysis was carried out by Bhat [52].

Table 8: Comparison of natural frequencies of SS beam.

Mode	Dynamic condensation.		Static load vectors in Rayleigh-Ritz.	
	Values (Hz.)	Equivalent mode	Values (Hz.)	Error (%)
1	117.2666	1	117.2666	0
2	469.0674	2	469.0674	0
3	1876.3471	4	1055.4135	0
4	9508.9999	9	1876.3471	0
5	108571.4592	29	2931.9771	0
6	293539.6389	43	4222.536	0
7	310537.3321	44	6131.0667	6.657
8	326820.6804	45	7610.4935	1.335
9	341733.1594	46	13731.573	44.4061
10	354516.9925	47	184179.71	1468.0

3.5.3. Clamped-clamped beam

Clamped-clamped beams are also studied using the modified Gram-Schmidt, orthogonal vectors generated as static deflection and the dynamic condensation. Fig. 20-22 show the comparison between the exact mode shapes of the structure with the assumed vectors for the Rayleigh-Ritz analysis. Again both methods show good resemblance to the exact mode shapes, however, in terms of results, the second method has better accuracy. Also it should be noted that the modified Gram-Schmidt method would be somewhat difficult in the case of two or three dimensional problems since it requires the coordinates of the nodes.

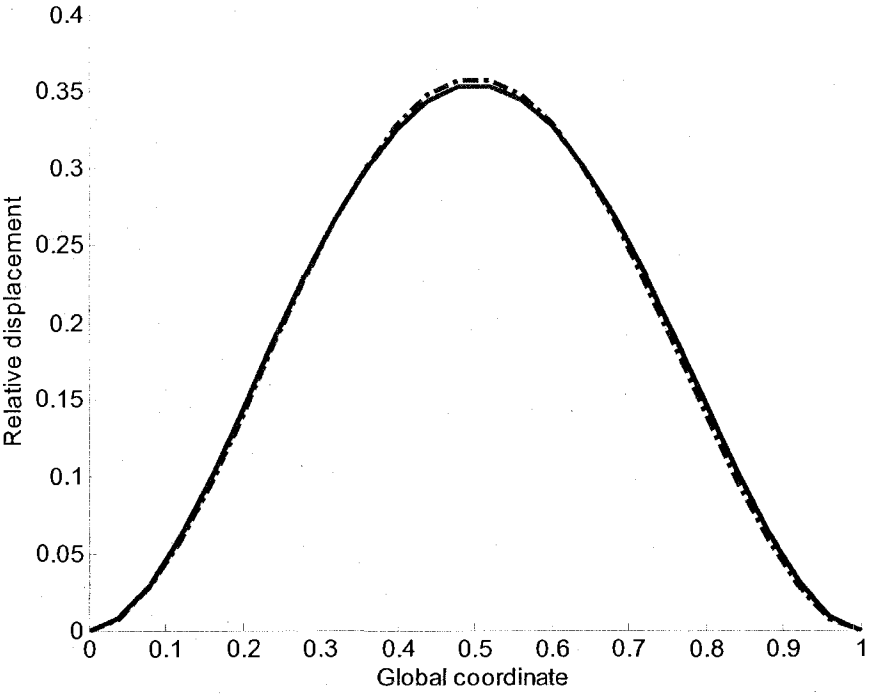

Fig. 20. Comparison of the first exact mode with assumed vectors. _____ Exact mode, _ _ _ _ _ _ _ modified Gram-Schmidt, _ . _ . _ . _ .static deflection vectors.

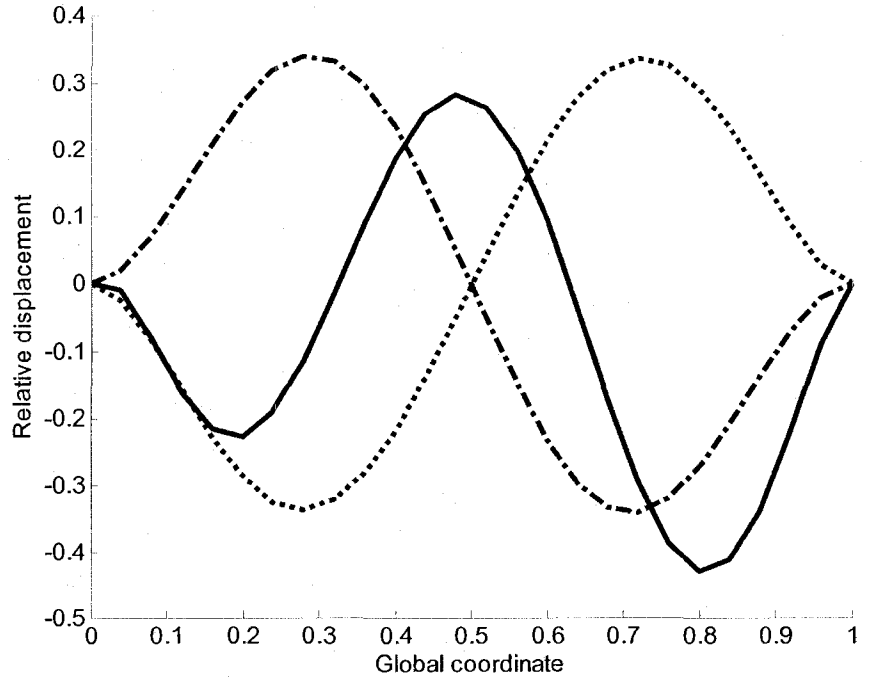

Fig. 21. Comparison of the third exact mode with assumed vectors. _____ Exact mode, _ _ _ _ _ _ _ modified Gram-Schmidt, _ . _ . _ . _ .static deflection vectors.

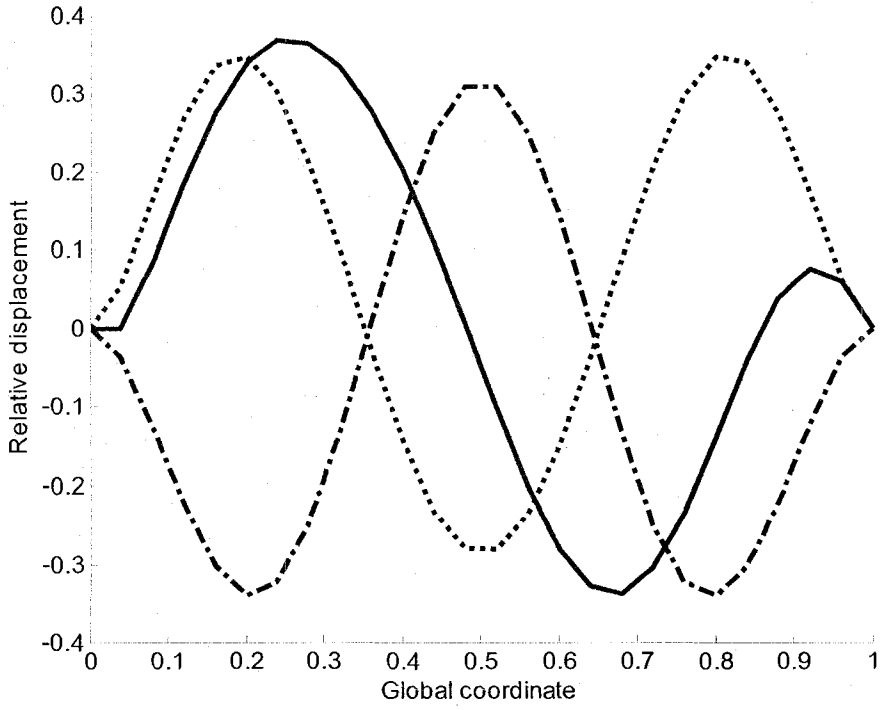

Fig. 22. Comparison of the fifth mode with assumed vectors. _____ Exact mode, _ _ _ _ _ _ _ modified Gram-Schmidt, _ . _ . _ . _ .static deflection vectors.

Table 9: Comparison between the reduced natural frequencies of different methods for CC beam.

Mode	Dynamic condensation.		Modified Gram-Schmidt.		Static load vectors in Rayleigh-Ritz.	
	Values (Hz.)	Error (%)	Value (Hz.)	Error (%)	Values (Hz.)	Error (%)
1	265.8303	(1) 0	277.1925	4.2742	265.8303	0
2	732.7758	(2) 0	744.5748	1.6102	732.7758	0
3	1436.5609	(3) 0	1449.6511	0.9112	1436.560	0
4	2374.8141	(4) 0	2389.7234	0.6278	2374.814	0
5	3547.868	(5) 0	3565.5399	0.4981	547.868	0
6	4956.0166	(6) 0	4982.0496	0.5253	4956.176	0.0032
7	6599.7745	(7) 0	6964.5501	5.5271	6674.132	1.1267
8	8479.9408	(8) 0	9181.6729	8.2752	8827.717	4.1012
9	55734.6248	(21) 0	16933.2757	59.7828	16682.32	57.4148
10	167160.9828	(34) 0	22612.2036	74.5493	277324.5	2040.73

Table 9 shows the comparison between the eigenvalues computed using different reduction methods for the clamped-clamped beam. The exact dynamic condensation will not show a significant error, however, it causes a loss of some modes with a poor choice of master DOFs. The modified Gram-Schmidt method shows acceptable results, however, it is computationally inconvenient in case of complex geometry. Finally the orthogonal vectors generated by the static deflection algorithm shows good results with a simple procedure. It should also be noted that both the exact dynamic and the static condensations require a rearrangement of the FEM matrices. That also may be computationally inconvenient. Moreover, the iterative nature of the solution of dynamic condensation requires a starting frequency, and may create the problem of repeated frequencies.

In this chapter, Gram Schmidt method was modified to deal with dependent degrees of freedom. Moreover, a new method of generation of the vectors is proposed and the formulation and the algorithm are presented. Static and dynamic condensation methods are presented and discussed. The latter two methods and the newly proposed ones are compared using FEM models for different beams. In the next chapter the method that employs the vectors generated as static deflections is applied to different case studies.

Chapter 4

Applications of the model reduction using orthogonal vectors set in the Rayleigh-Ritz method.

4.1. Introduction

In chapter 3, the newly proposed method of model reduction by boundary characteristic orthogonal vectors was investigated and the results were compared with earlier studies. In this chapter the application of this method on different case studies will be carried out. First a model of a vehicle system with components having distributed mass and elasticity as well as attached discrete degrees of freedoms will be studied, and then a coiled heat exchanger meshed in ANSYS.

In the first case the main interest is to find the mode shapes of the vehicle model and its harmonic response. The vehicle is modeled as a flexible beam with two spring damper mass systems attached to it. The vehicle itself is also elastically connected to the ground through which it receives some disturbances. It should be noted that the damping coefficients for the discrete dampers are taken into account, however, no structural damping is considered for the chassis beam.

The second case is an investigation to obtain the natural frequencies of a coiled heat exchanger proposed by Kumar, et al. [56]. This model is meshed into three dimensional elements including 6 DOF at each node. The resulting matrices are reduced and the

eigenvalue results are compared with those of the complete FEM model of the system. The mass of the fluid contained in a beam element is simply added to the mass of the beam element itself, however, the flow effect of the fluid are not considered.

4.2. Harmonic analysis of vehicle reduced order model

In this section, a vehicle hybrid model consisting of a combination of discrete and continuous subsystems is analyzed. The discrete subsystems represent the human body and the engine as two masses elastically connected to the chassis. The continuous subsystem represents the chassis of the vehicle that is modeled as a beam. The FEM modeling of this structure is done using a MATLAB program. The constraints applied on the system represent the wheel contacts. Fig. 23 shows the model of the vehicle used for the study. The two attached masses are constrained to move vertically.

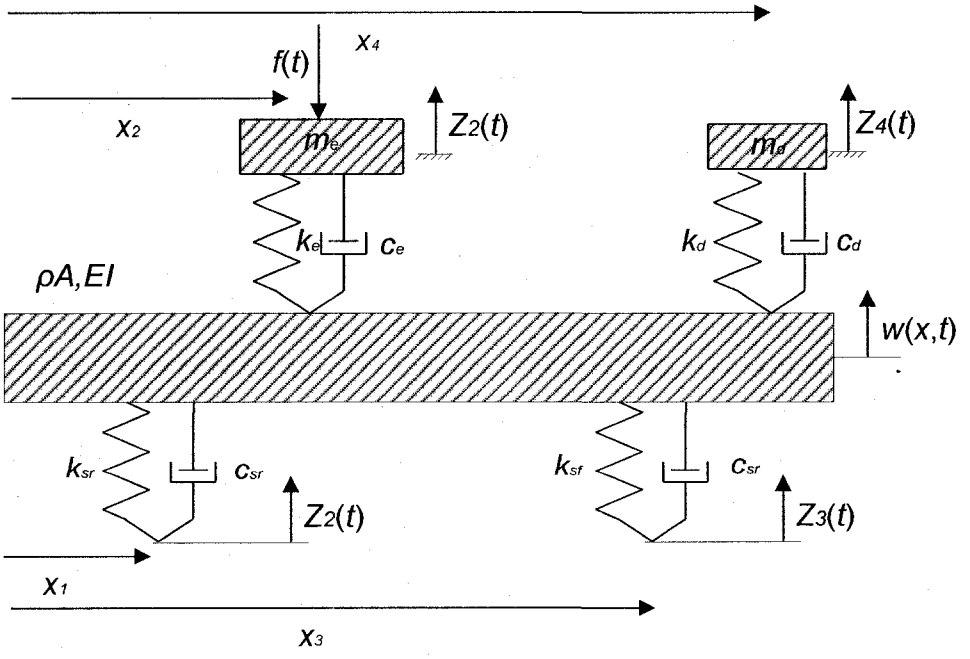

Fig. 23. Vehicle body model with attached spring mass systems.

The finite element model of the system shown in the above figure was constructed using one dimensional bending beam elements and lumped masses elastically attached to the chassis for the discrete blocks. Hence the attached masses constitute two additional nodes. The model is made of a total of 125 nodes where only the last 4 correspond to the rear wheel, front wheel, engine and driver, respectively. The resultant FEM model yields a total of 246 DOFs.

Those DOF are precisely formed of 121 translational and rotational degrees of freedom along the beam, and 4 translational degrees of freedom for the four connected spring mass systems. The length of the elements is taken to be 0.1 m. Hence the engine is connected at the node number 61 and the driver is connected at node 111. Nodes 122 and 123, corresponding to the wheels, are assumed to keep contact with the ground. This assumption is equivalent of replacing the nodes with two pins. The locations of the most important nodes are given in Fig. 24.

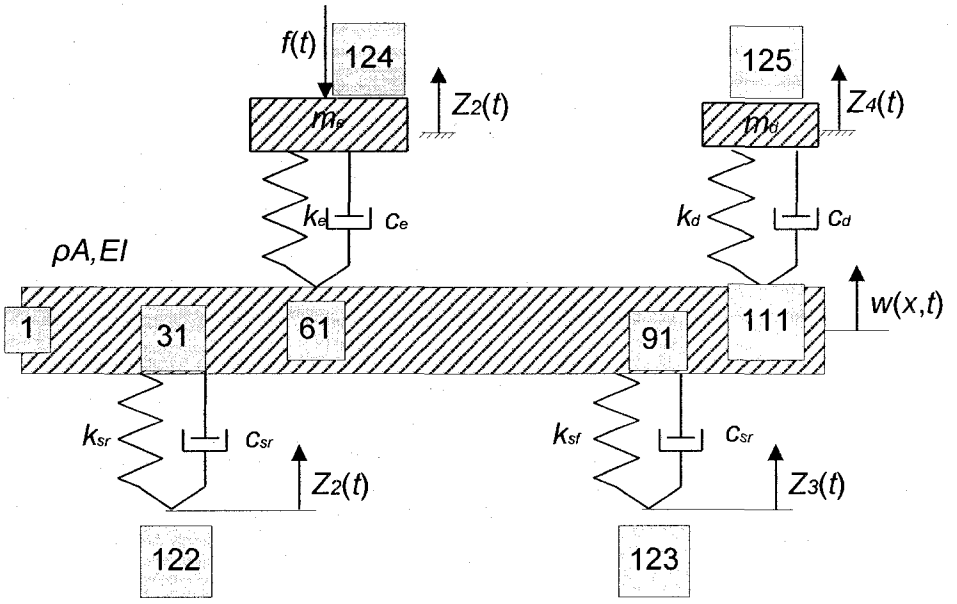

Fig. 24. Node location of FEM model.

The parameters used in the study are given in Table 10. These Parameters correspond to a city bus and have been taken from [53-55], and those that are not found in [53-55] have been estimated.

Table 10: Numerical parameters.

Parameter	Value	Unit
L	12	m
x_1	3	m
x_2	1	m
x_3	9	m
x_4	11	m
k_{sr}	280	kN/m
k_{sf}	240	kN/m
k_d	10500	N/m
k_e	140	kN/m
c_{sr}	4	kN.s/m
c_{sf}	7	kN.s/m
c_d	830	N.s/m
c_e	800	N.s/m
m_d	70	kg
m_e	3600	kg
ρA	1000	kg/m
EI	1	MNm^2

The reduced model is obtained using ten orthogonal vectors, resulting in (10×10) eigenvalue problem. The eigenvalues of the reduced model are calculated and compared with the exact ones in Table 11. The computed values show a good agreement with those for the complete system model. The eigenvalues for the reduced 10 DOF model agree with those of the complete model with an accuracy up to the 4^{th} decimal place until the 6^{th}

natural frequency and then slowly start increasing for the higher ones as expected. The last two values are far higher than those for the complete model.

Table 11: Comparison of exact and reduced natural frequencies.

Mode	Natural Frequencies		Error (%)
	Reduced	Exact	
1	0.7075	0.7075	0
2	0.8906	0.8906	0
3	1.1888	1.1888	0
4	1.9039	1.9039	0
5	2.5674	2.5674	0
6	6.9303	6.9303	0
7	13.4438	13.4434	0.003
8	22.0986	22.098	0.0027
9	46.6682	33.0111	41.3715
10	127.3379	46.1088	176.1685

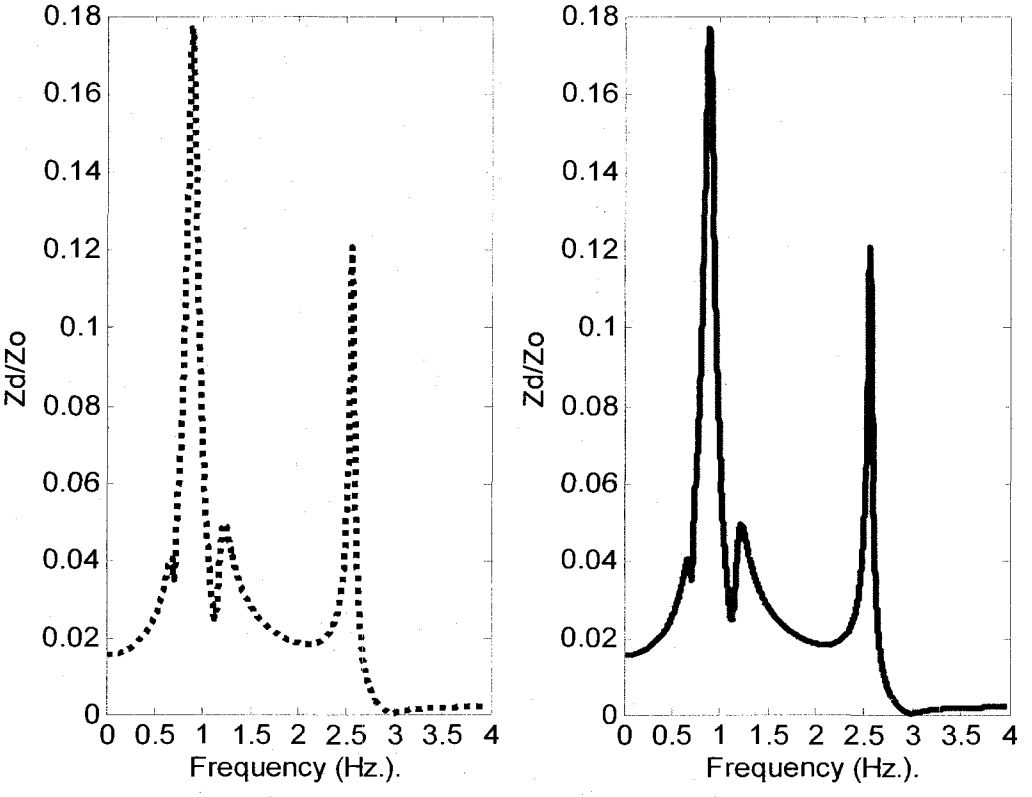

Fig. 25. Transmissibility plots of the exact and reduced models. _____ Exact model, _ _ _ _ _ _ _ reduced model.

Fig. 25 and 26 show the transmissibility and phase plots, respectively, of the vehicle subjected to a harmonic excitation with an amplitude of 0.1 m at the front wheel. In the current study, the focus is on the ability of the proposed model reduction technique to predict the natural frequencies and the response behavior. Both figures show that the reduction has given very good results. It should be noted that the plots are separated into two windows because one overlaps the other when plotted together in the same window. Moreover the "clock" command in MATLAB was used to measure the computational time. It is found that finding the transmissibility plots using the exact model requires 118.1870 sec, while generating the orthogonal vectors and reducing the system in order to finally obtain the transmissibility plots have only taken 0.5 sec, which proves the significant benefit of model reduction.

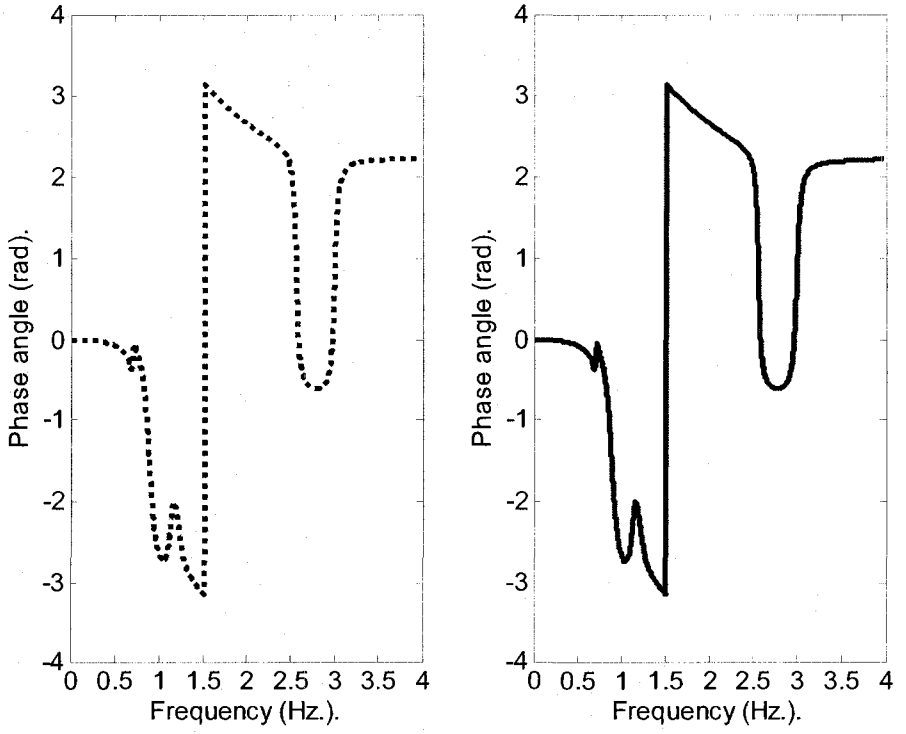

Fig. 26. Phase plots of the exact and reduced models. _____ Exact model, - - - - - - - reduced model.

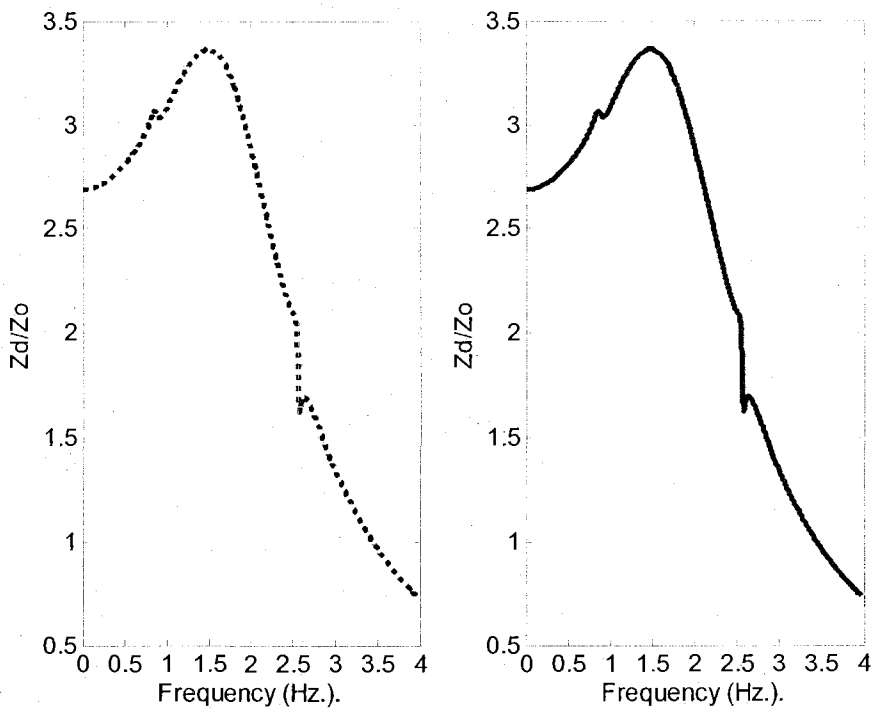

Fig. 27. Transmissibility plots of exact and reduced models. _____ Exact model, _ _ _ _ _ _ _ reduced model.

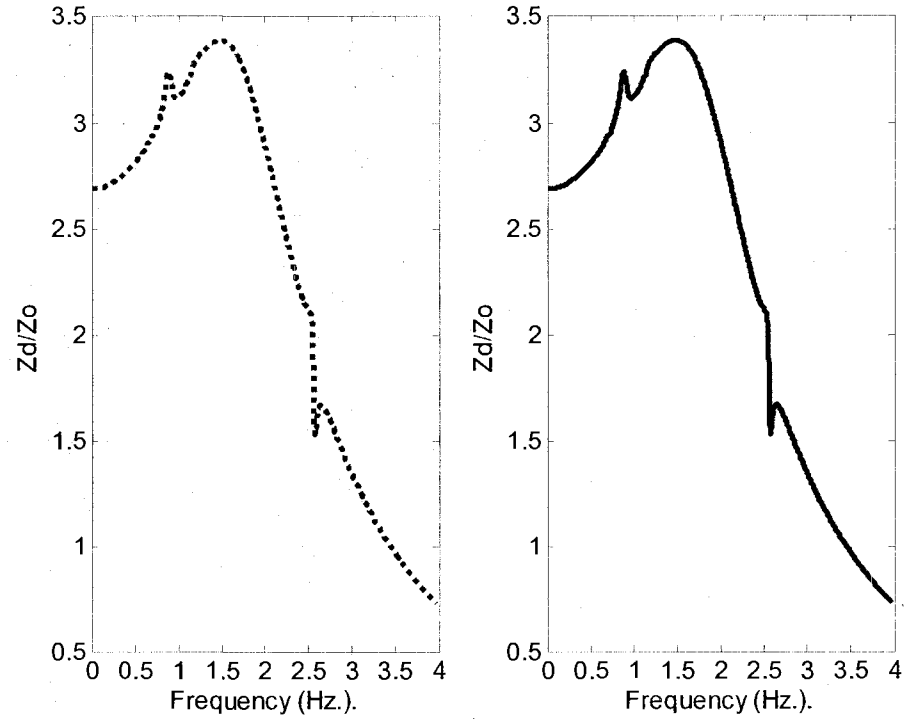

Fig. 28. Transmissibility plots of exact and reduced models. _____ Exact model, _ _ _ _ _ _ _ reduced model.

Fig. 27 and 28 show the transmissibility plots due to a harmonic excitation to the rear wheel and to both the wheels, respectively. Those plots also show the capability of the reduced order model to approximate the response to a harmonic excitation with a great saving in the computational effort.

4.3. Model reduction of a fluid filled pipe

The proposed model reduction technique is applied on a three dimensional structure of a coiled pipe heat exchanger filled with water. The model is used to simulate the vibration behavior of the coiled heat exchanger proposed in [56]. The original structure is made of 8 identical banks, one of which is shown in Fig. 29.

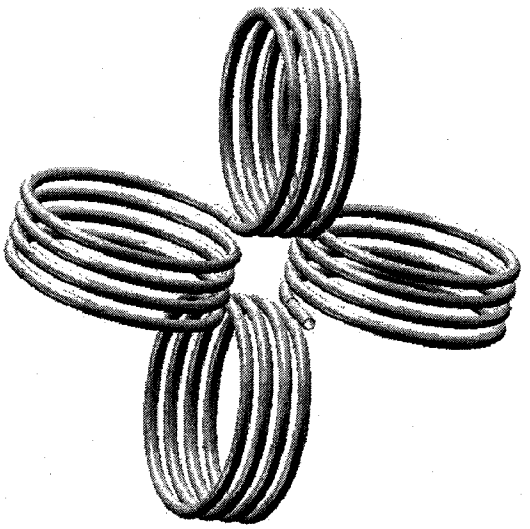

Fig. 29. Sketch of one bank of the coiled heat exchanger.

4.3.1. Modeling using FEM

The modeling of the structure is done in two parts. First the structure is plotted in MATLAB, and the coordinates are transferred to ANSYS where the model is created and meshed. The resulting matrices are taken from ANSYS to MATLAB in order to perform necessary matrix operations for the reduction.

Initially, the coiled heat exchanger is represented by a total of four 3D curves. Those curves are made from parametric equations containing two terms as trigonometric functions while the last is linear along a direction. The general form of those equations are shown below,

$$\begin{aligned} x &= a_1 t \\ y &= a_2 \sin(t) \\ z &= a_3 \cos(t) \end{aligned} \tag{4.1}$$

The four exact functions used in this case are shown in Table 12. As seen, the equations are linear either along x or y which coincides with the axis of the circular coil. And the minus sign that multiplies t in some equations is appearing because the structure is going backward at the definite bend.

Fig. 30 shows the representation of the bank shown in Fig. 29, using the parametric equations presented in Table 12.

Table 12: Parametric equations of the coil.

Bend Number	Equation
1. Linear with x and rotating around it.	$\begin{cases} x = 0.0032t \\ Y = 0.102\sin(t) \\ z = 0.102\cos(t) \end{cases}$
2. Linear with y and rotating around it.	$\begin{cases} x = 0.102\sin(t) + 0.1824 \\ y = 0.102\cos(t) \\ z = 0.0032t + 0.1070 \end{cases}$
3. Linear with x and rotating around it.	$\begin{cases} x = -0.0032t + 0.0855 \\ y = -0.102\cos(t) \\ z = -0.102\sin(t) + 0.2844 \end{cases}$
4. Linear with y and rotating around it.	$\begin{cases} x = 0.102\sin(t) - 0.1020 \\ y = -0.102\cos(t) \\ z = -0.0032t + 0.1875 \end{cases}$

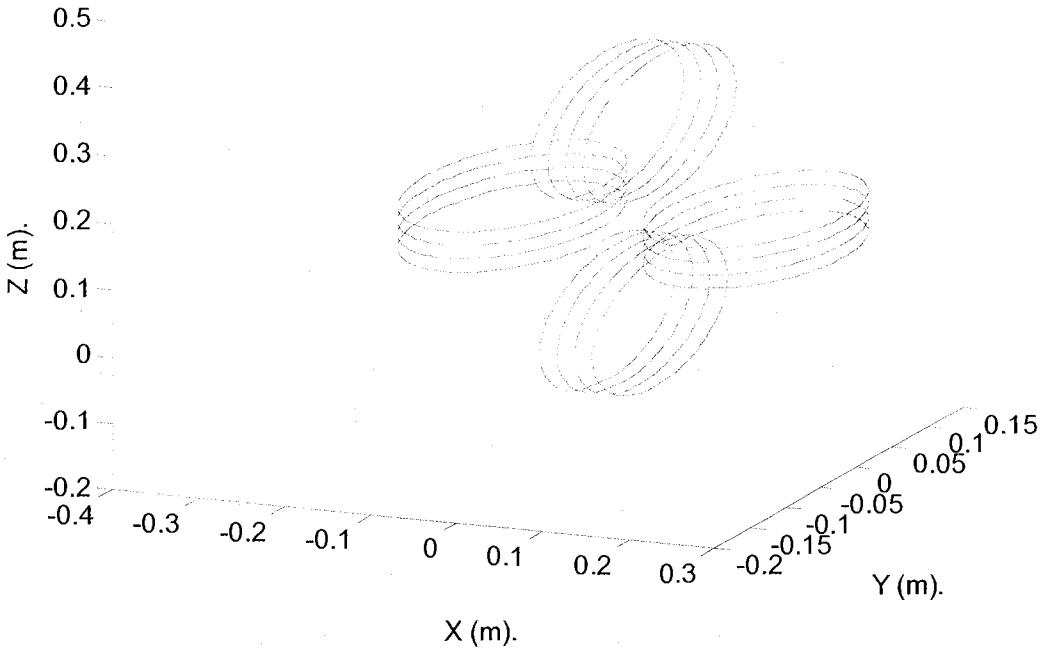

Fig. 30. The simulation of the coil bank by a 3D curve.

Fig. 31 shows the simulation of the coil bank using the set of parametric equations presented in Table 12. The smoothness of this curve is ensured by taking a small increment of t. While in case of Fig. 31, the increment is taken as $\pi/4$ and the resulting components of each point are stored since those will form the geometry input to ANSYS. As shown in Fig. 31, as well, the chosen increment does not result in the distortion of the geometry. The operated mesh in MATLAB has resulted in a total of 128 elements and 129 nodes, resulting in 774 DOFs with 6 DOFs at each node. The geometry and properties of the coil are shown in Table 13.

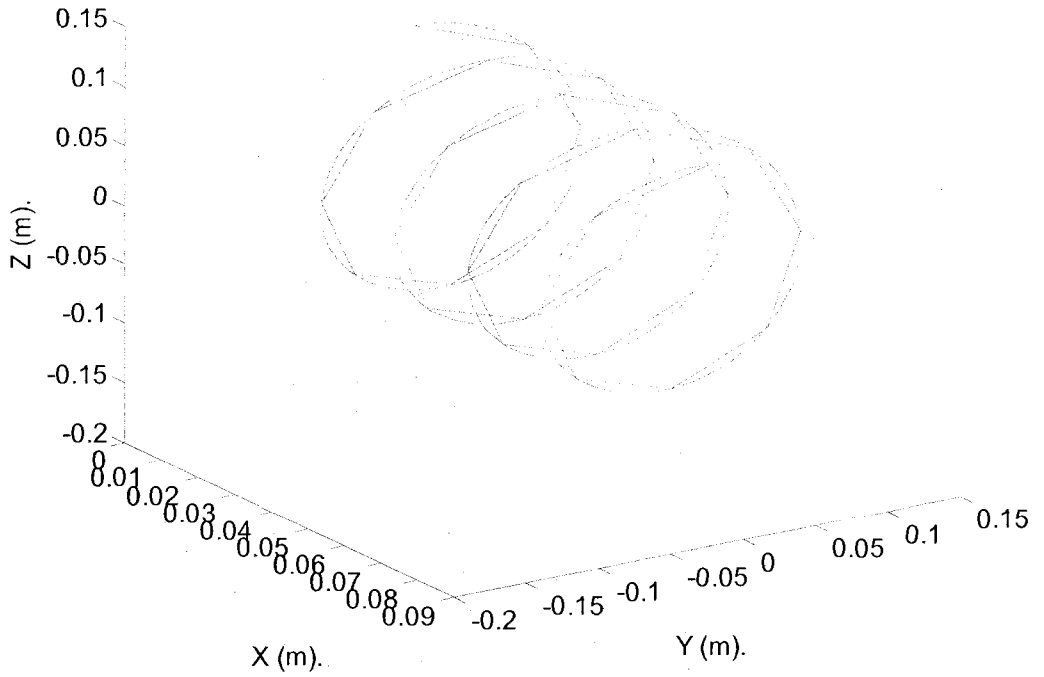

Fig. 31. Exact vs. meshed models.

Table 13: Geometry and parameters of the coil.

Outer diameter	12.7	mm
Wall thickness	1.2	mm
Radius of curvature of the coil	102	mm
Pitch of the coil	20	mm
Modulus of elasticity of pipe Material	193	Mpa
Shear modulus of pipe material	78	Mpa
Mass per unit length of the pipe	0.3481	Kg/m
Mass per unit length of the fluid	0.0833	Kg/m

4.3.2. Reduction of the model

The model is assumed to be supported at nodes, 65, 73, 81, 89 and 97, where the coil is constrained in all directions. The positions of those nodes are shown in Fig. 32.

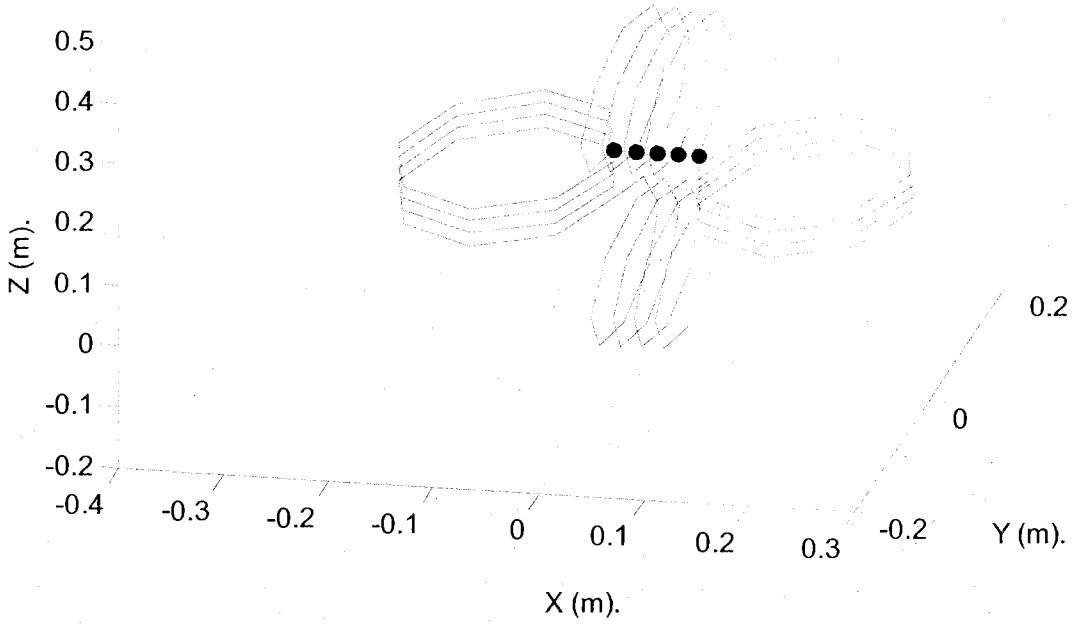

Fig. 32. Support locations.

Two cases of reduction are performed; one using 10 orthogonal vectors and the second using 20 of them. The resulting natural frequencies are compared with the complete model solution.

Table 14: Eigenvalue of reduced (10 natural frequencies) and complete model.

Modes	Reduced Model (Hz.)	FEM (Hz.)	Error (%)
1	0.9118	0.9118	0
2	3.2692	3.2692	0
3	3.4524	3.4524	0
4	6.2023	6.2023	0
5	6.9675	6.9675	0
6	9.9033	9.9012	0.021
7	12.0092	10.0158	20.80
8	16.8893	11.9989	40.76
9	25.3808	16.4953	53.87
10	47.8071	19.2100	148.86

Table 15: Eigenvalue of reduced (20 natural frequencies) and complete model.

Modes	Reduced Model (Hz.)	FEM (Hz.)	Error (%)
1	0.9118	0.9118	0
2	3.2692	3.2692	0
3	3.4524	3.4524	0
4	6.2023	6.2023	0
5	6.9675	6.9675	0
6	9.9012	9.9012	0
7	10.0158	10.0158	0
8	11.9989	11.9989	0
9	16.4953	16.4953	0
10	19.2100	19.2100	0
11	20.6708	20.6704	0.0018
12	22.8776	22.5287	1.5487
13	24.9467	22.9538	8.6819
14	27.9811	25.2499	10.8164
15	30.3406	28.8345	5.2234
16	37.4754	30.0403	24.7504
17	43.9935	31.6851	38.8461
18	56.2358	32.7026	71.961
19	82.1543	35.3791	132.2116
20	437.6680	37.6601	1062.1524

Table 14 and Table 15 show the reduced natural frequencies and their comparison with those from the complete FEM model. It is shown in both cases that this method is capable of approximating around half of the reduced order model results with negligible error.

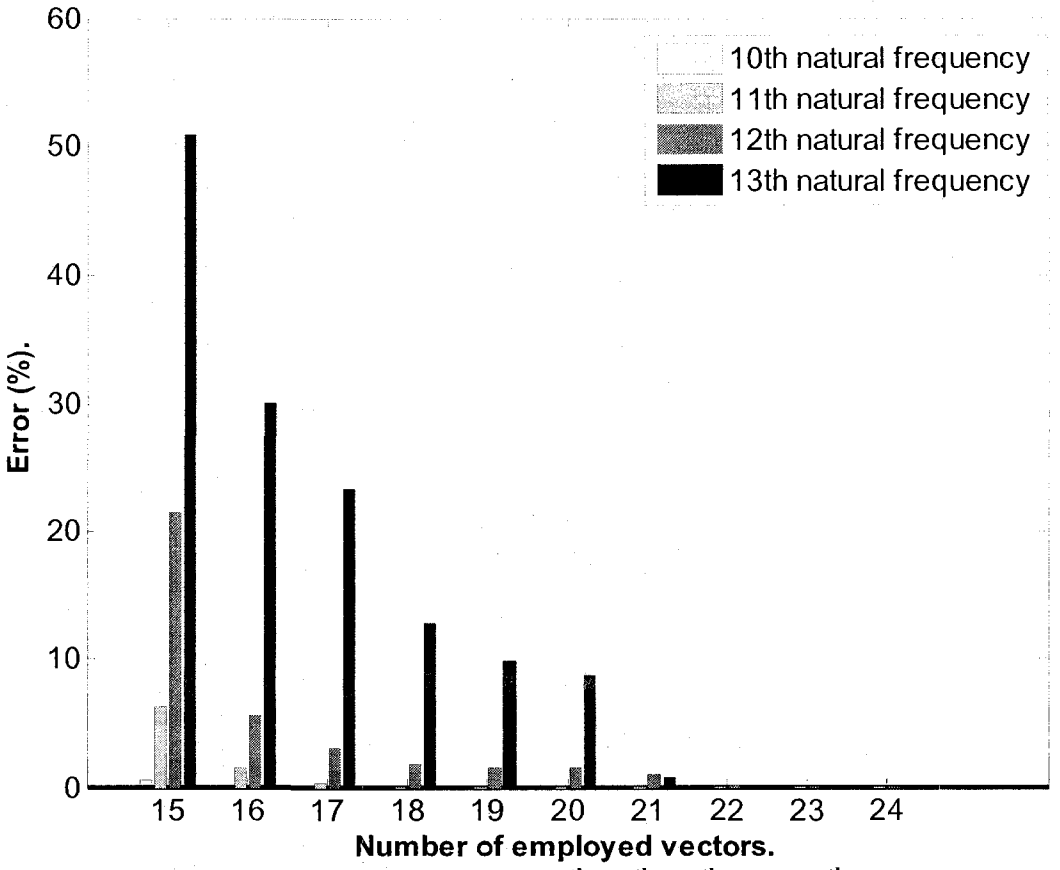

Fig. 33. Convergence history of 10^{th}, 11^{th}, 12^{th}, and 13^{th} modes.

Fig. 33 shows the convergence history of 10^{th} to 13^{th} modes versus the number of employed vectors. As seen before in Table 14 and Table 15, the higher order of the reduced model eigenvalues have poor values with large errors. This convergence history plot shows that the 13^{th} natural frequency converges toward that of the complete model when a total of 22 vectors are employed. Hence the number of employed vectors should be larger than the number of desired modes to secure a better convergence at the higher modes of the reduced model.

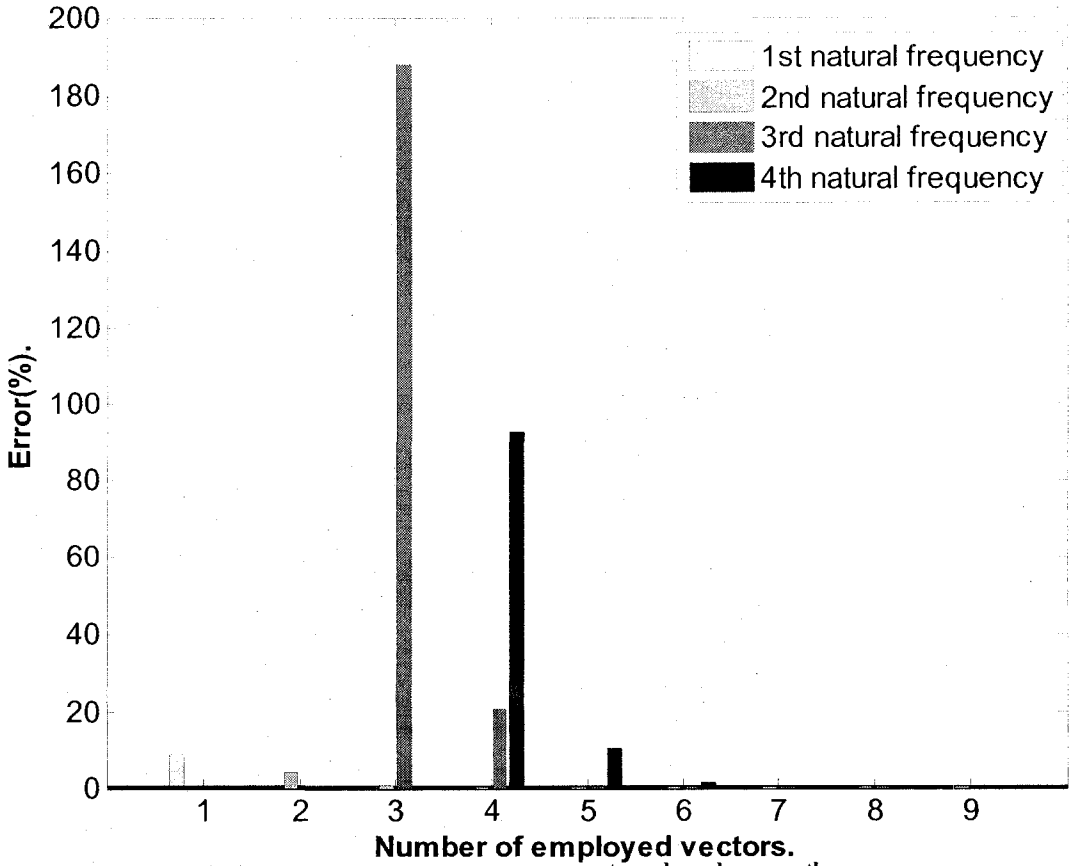

Fig. 34. Convergence history of 1st, 2nd, 3rd and 4th modes.

Fig. 34 shows the convergence history of the 1st to 4th modes. When only one vector is used, one bar can be noticed which represents the error at the 1st natural frequency. On the other hand when two vectors are used, it should be noted that two bars corresponding to the error at the 1st and the 2nd natural frequencies must be represented. However only the latter is shown since the former have already converged to zero. When the number of used vectors reaches 4 the number of bars will remain 4 afterward, since the convergence of only the firt four natural frequencies is studied. Note that when 7 vectors are used in the study the error is almost zero in all the 4 modes.

In this chapter the proposed model reduction method is applied on two models of a vehicle and a coiled pipe, respectively. The orthogonal vectors are the physical static deflection due to a load distibution. However, a set of vectors that are calculated in a similar manner can be used to solve any system of equations. In these cases, the vectors will be a generalized coordinate vector. In the coming chapter, the Rayleigh-Ritz method with orthogonal polynomial functions in two dimensions are used to solve problem of an elliptical plate. The resulting generalized stiffness and mass matrices are reduced using the newly proposed algorithm.

Chapter 5

Using independent vectors for the reduction of generalized eigenvalue problem

The boundary characteristic orthogonal vectors were calculated in previous chapters as the static defflections due to loads proportional to the preceding assumed deflection shapes. In this chapter the coeficients of the assumed functions are considered as generalized coordinates and the reduction is done on the number of the new generalized coordinates used in the reduced model. The case of an elliptical plate is studied using two dimensional orthogonal polynomials in the Rayleigh-Ritz method.

A systematic method of generating the admissible functions of arbitrary clamped plates with different shapes is presented. The method of orthogonalization is similar to that proposed by Staib [29].

5.1. The Rayleigh-Ritz method for plate vibrations

As mentioned earlier the Rayleigh-Ritz method requires the expressions of the energy. For the plate case the kinetic and strain energy expressions are shown in Eq. (5.1) and (5.2), respectively. Note that, $w(x,y)$ is replaced by w and a, b and h are the dimensions of the plate in x, y and z directions, respectively, and $D = Eh^3 / 12(1-\nu^2)$ is the flexural rigidity. The boundaries of the integrals are defined by the geometry of the plate.

$$T_{\max} = \frac{1}{2}\rho h\omega^2 \iint w^2 dxdy \tag{5.1}$$

$$U_{\max} = \frac{1}{2}D\iint\left[\left(\frac{\partial^2 w}{\partial x^2}\right)^2 + \alpha^4\left(\frac{\partial^2 w}{\partial y^2}\right)^2 + 2\nu\left(\frac{\partial^2 w}{\partial x^2}\right)\left(\frac{\partial^2 w}{\partial y^2}\right) + 2(1-\nu)\left(\frac{\partial^2 w}{\partial x \partial y}\right)^2\right]dxdy \tag{5.2}$$

The deflection is expressed as a sum of assumed mode shapes $\varphi_m(x,y)$ as shown below:

$$w(x,y) = \sum_m \varphi_m(x,y) q_m \tag{5.3}$$

Introducing the non dimensional parameters, $\alpha = \frac{a}{b}$, $\xi = \frac{x}{a}$, $\eta = \frac{y}{b}$ in Eq. (5.3):

$$w(\xi,\eta) = \sum_m \varphi_m(\xi,\eta) q_m \tag{5.4}$$

Substituting Eq.(5.4) in Eqs. (5.1) and (5.2) results in the following two equations, respectively:

$$T_{\max} = \frac{1}{2}\rho hab\omega^2 \iint w^2 d\xi d\eta \tag{5.5}$$

$$U_{\max} = \frac{1}{2}D\frac{ab}{a^4}\iint\left[\left(\frac{\partial^2 w}{\partial \xi^2}\right)^2 + \alpha^4\left(\frac{\partial^2 w}{\partial \eta^2}\right)^2 + 2\nu\alpha^2\left(\frac{\partial^2 w}{\partial \xi^2}\right)\left(\frac{\partial^2 w}{\partial \eta^2}\right) + 2(1-\nu)\alpha^2\left(\frac{\partial^2 w}{\partial \xi \partial \eta}\right)^2\right]d\xi d\eta \tag{5.6}$$

Using the stationarity condition of the Rayleigh's quotient results in the following eigenvalue problem:

$$\frac{\partial U_{\max}}{\partial q_n} - \lambda^2 \frac{\partial T_{\max}}{\partial q_n} = 0 \quad for\ n = 1,2,...,N. \tag{5.7}$$

where, N is the number of assumed mode shapes and $\lambda^2 = \frac{\rho h \omega^2 a^4}{D}$ is the non-dimensional eigenvalue. Eq. (5.7) can be rewritten as a matrix eigenvalue problem as follows:

$$\sum_i \sum_j \left[K_{ij} - \lambda^2 M_{ij} \right] q_i = 0 \tag{5.8}$$

where,

$$K_{ij} = \iint \left(\frac{\partial^2 \varphi_i}{\partial \xi^2} \right) \left(\frac{\partial^2 \varphi_j}{\partial \xi^2} \right) d\xi d\eta + \alpha^4 \iint \left(\frac{\partial^2 \varphi_i}{\partial \eta^2} \right) \left(\frac{\partial^2 \varphi_j}{\partial \eta^2} \right) d\xi d\eta$$
$$+ 2\nu\alpha^2 \iint \left(\left(\frac{\partial^2 \varphi_i}{\partial \xi^2} \right) \left(\frac{\partial^2 \varphi_j}{\partial \eta^2} \right) + \left(\frac{\partial^2 \varphi_j}{\partial \xi^2} \right) \left(\frac{\partial^2 \varphi_i}{\partial \eta^2} \right) \right) d\xi d\eta$$
$$+ 2(1-\nu)\alpha^2 \iint \left(\frac{\partial^2 \varphi_i}{\partial \xi \partial \eta} \right) \left(\frac{\partial^2 \varphi_j}{\partial \xi \partial \eta} \right) d\xi d\eta,$$

$$M_{ij} = \iint \varphi_i \varphi_j d\xi d\eta$$

Eq. (5.8) can also be written in $(N \times N)$ generalized matrix form, $\left[\hat{K} \right] - \lambda^2 \left[\hat{M} \right] = 0$. This form is that which will be reduced using the orthogonal vectors matrix transformation.

5.2. Assumed deflection shapes

The conditions at a clamped support are that the deflection and slope are zero. The first deflection shape is assumed as the simplest function that satisfies the geometrical boundary conditions. These conditions at an arbitrary support $F(\xi,\eta)$ are shown below:

$$\varphi_1|_{F(\xi,\eta)} = 0, \quad \left.\frac{\partial\varphi_1}{\partial\xi}\right|_{F(\xi,\eta)} = 0, \quad \left.\frac{\partial\varphi_1}{\partial\eta}\right|_{F(\xi,\eta)} = 0 \tag{5.9}$$

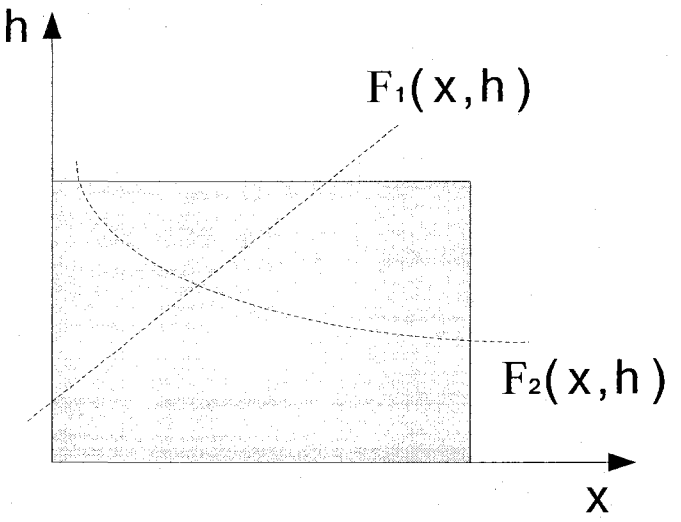

Fig. 35. General plot of a rectangular plate with line supports.

A function that can satisfy the conditions of Eq. (5.9) can be found as:

$$\varphi_1(\eta,\xi) = F^2(\xi,\eta) \tag{5.10}$$

The fact that this shape function satisfies the listed condition can easily be proved by differentiating in both directions. In case of multiple supports as in Fig. 35 the first shape function can be taken in the following form:

$$\varphi_1(\eta,\xi) = F_1^2(\xi,\eta) F_2^2(\xi,\eta) \tag{5.11}$$

The orthogonality condition used for the orthogonalization procedure can be defined in view of the nature of the problem. For example the case of nonhomogonous structures can be studied using a weight function in orthogonalization. In the present case the plate is uniform and the orthogonality condition is taken as follows:

$$\int\int \varphi_i \varphi_j d\xi d\eta = 0 \tag{5.12}$$

In order generate the rest of the functions, a linear independent basis Φ of a vector space V is created by multiplying the first functions by $\xi^r \eta^s$, following the sequence shown in Fig. 36.

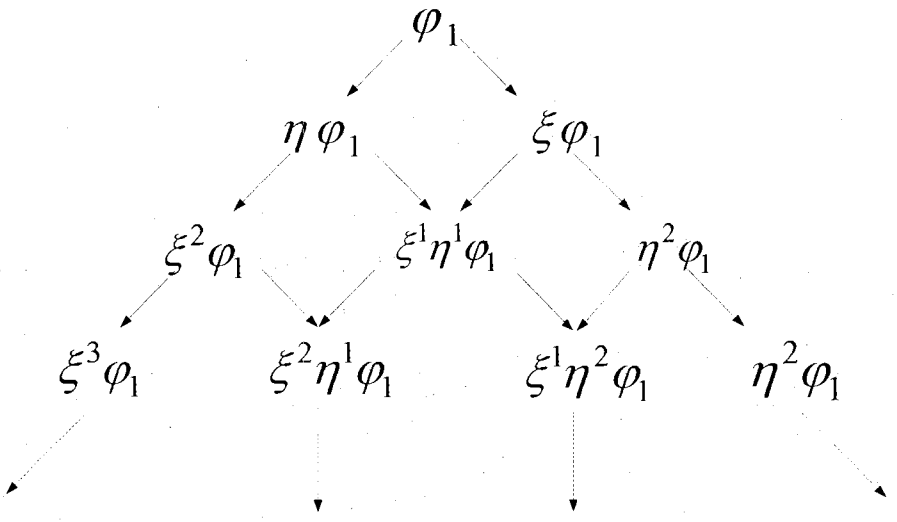

Fig. 36. Scheme of generating the linear independent basis.

The inner product in the space V is defined as follows:

$$\left(\varphi_i \square \varphi_j\right) = \int\int \varphi_i \varphi_j \, d\xi d\eta \tag{5.13}$$

The boundaries of the integration are defined by the plate in study. The inner product matrix representation of the basis Φ is obtained as follows:

$$B_{ij} = \int\int \varphi_i \varphi_j \, d\xi d\eta \tag{5.14}$$

where φ_i and φ_j are, respectively, the i^{th} and j^{th} element of Φ, and B_{ij} are the elements of $[B]$. It can be easily seen that $[B]$ is symmetric. Eq. (5.3) can be rewritten in the following form:

$$W_1 = \sum_{i=1}^{n} \varphi_i q_{1,\Phi}^i = [\Phi]^T \{q_{1,\Phi}\} \tag{5.15}$$

where $q_{1,\Phi}$ is the Φ coordinate representation of W_1. Thus, W_2 can be written as follows:

$$W_2 = [\Phi]^T \{q_{2,\Phi}\} \tag{5.16}$$

Using the two previous equations, the inner product of two arbitrary shape functions can be obtained as follows:

$$W_1 \square W_2 = \int_a^b \int_a^b \left(\sum_{i=1}^{n} \varphi_i q_{1,\Phi}^i \right) \left(\sum_{i=1}^{n} \varphi_i q_{2,\Phi}^i \right) \tag{5.17}$$

Rearranging Eq. (5.17) yields:

$$W_1 \square W_2 = \sum_{i=1}^{n} \sum_{j=1}^{n} q_{1,\Phi}^i \left(\int_a^b \int_a^b \varphi_i \varphi_j \right) q_{1,\Phi}^j = \sum_{i=1}^{n} \sum_{j=1}^{n} q_{1,\Phi}^i \left(B_{ij} \right) q_{1,\Phi}^j \tag{5.18}$$

It is easy to see that Eq. (5.18) can be written as follows:

$$(W_1 \square W_2) = \left[q_{1,\Phi} \right]^T [B] \left[q_{2,\Phi} \right] \tag{5.19}$$

Knowing that any space may have many ordered basis, the goal is to find another orthogonal ordered basis β. Let $q_{1,\beta}$ and $q_{2,\beta}$ be the representative β of the any deflection function. Defining the relation between the coordinate representation of Φ and β to be as follows:

$$q_\Phi = [A]^T q_\beta \tag{5.20}$$

Thus,

$$q_{1,\Phi} = [A]^T q_{1,\beta} \tag{5.21}$$

$$q_{2,\Phi} = [A]^T q_{2,\beta} \tag{5.22}$$

Using Eq. (5.21) and Eq. (5.22), Eq. (5.19) can be written as follows:

$$(W_1 \square W_2) = \left([A]^T q_{1,\beta}\right)^T [B]\left([A]^T q_{2,\beta}\right) = q_{1,\beta}^T \left([A][B][A]^T\right) q_{2,\beta}^T = q_{1,\beta}^T \left([D]\right) q_{2,\beta}^T \tag{5.23}$$

From the previous equation we can say that if the matrix $[D]$ is diagonal, then the basis β is an orthogonal basis. From linear algebra, the change of basis matrix is equal to the inverse of the transpose of the change of coordinate matrix. Thus, knowing that the transformation matrix in this case is $[A]^T$ as shown in equation (5.20), the two ordered basis are related by the following equation:

$$\Phi = \left[\left([A]^T\right)^T\right]^{-1} \beta \tag{5.24}$$

hence,

$$\beta = [A]\Phi \tag{5.25}$$

A process, similar to that of finding the inverse of a matrix, is used in order to find $[A]$ matrix. The Identity matrix is augmented to B matrix. The matrix B is transformed to an upper triangular matrix by a set of row operations, while the added identity matrix will be

converted to a lower triangular matrix. The proof that matrix $[A]$ satisfies the desired conditions is found in appendix-A.

5.3. Numerical result for elliptical plate

The case of elliptical plate is studied and the resulting stiffness and mass matrices are reduced using the newly proposed method in chapter 4. In this case a total of 25 functions were used and the generalized stiffness and mass matrices are of the size (27×27). These matrices are reduced to a (10×10) different generalized matrices.

Fig. 37 shows the assumed mode shapes obtained from the process explained in previous section. As shown, those plots can be arranged in four different groups:

- Symmetric about x-axis and y-axis (SS): 1, 4, 6, 11, 13, 15…
- Symmetric about x-axis and anti-symmetric about y-axis (SA): 3, 8, 10…
- Anti-symmetric about x-axis and symmetric about y-axis (AS): 2, 7, 9, 16…
- Anti-symmetric about x-axis and y-axis (AA): 5, 12, 14…

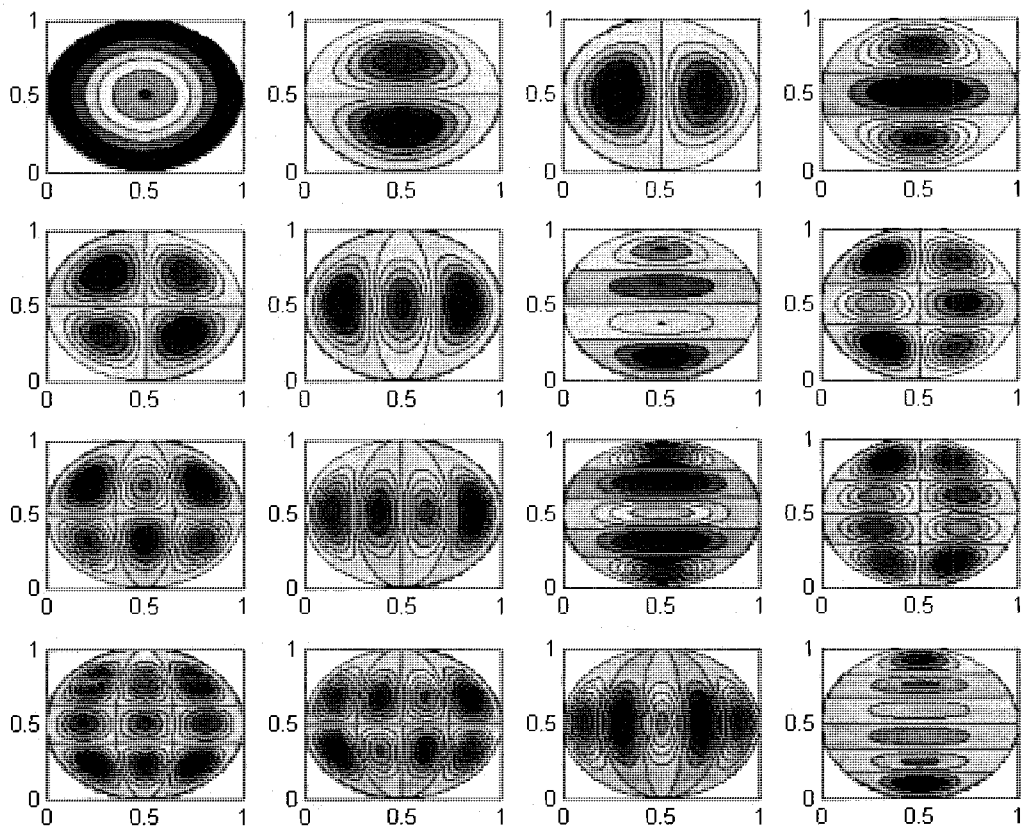

Fig. 37. Assumed mode shapes for elliptical and circular plates.

The plots shown in Fig. 37 are used for all elliptical plates since in the current formulation due to the introduction of the non-dimensional parameters all the ellipses are mapped on a circle. The ellipse is defined by the ratio of the major to minor axis, $\alpha = \frac{a}{b}$.

Fig. 38 shows the mode shapes of circular plates, for $\alpha = 1$. It is also seen that the resulting modes can be distinguished by the same criteria used to group the assumed ones. However, in the present case the (SA) and (AS) modes are merged to form one group. This is justified by the rotation of the axis of symmetry in those modes. Thus, if the plots are rotated to align the axis it can be seen that they are the same.

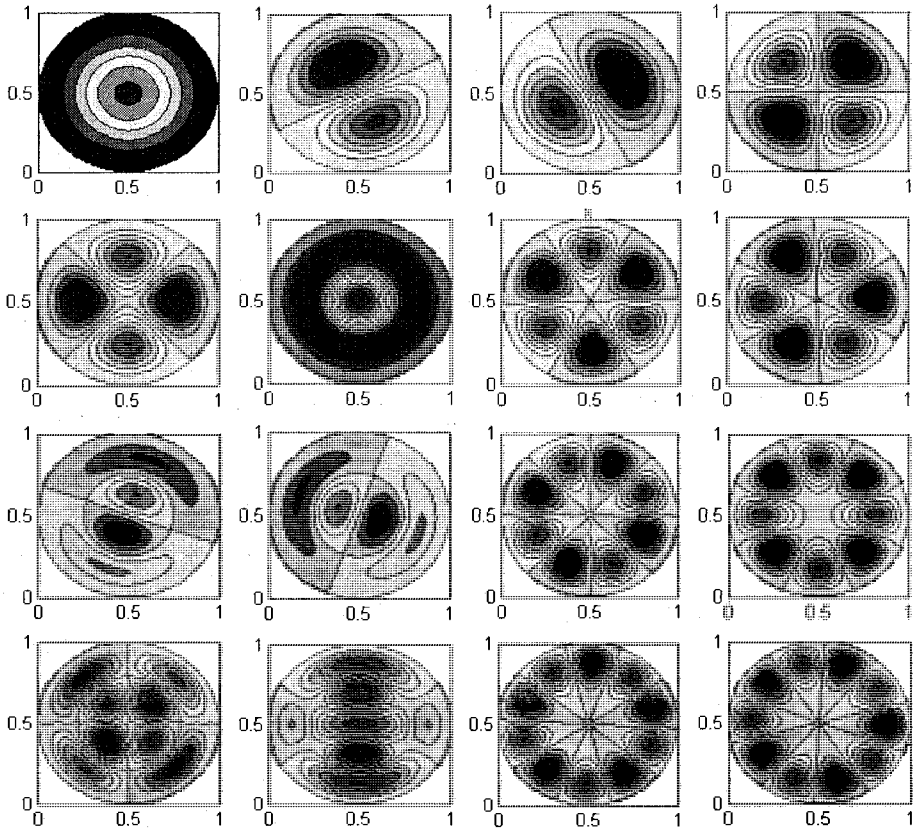

Fig. 38. Mode shapes of circular plates $\alpha = 1$.

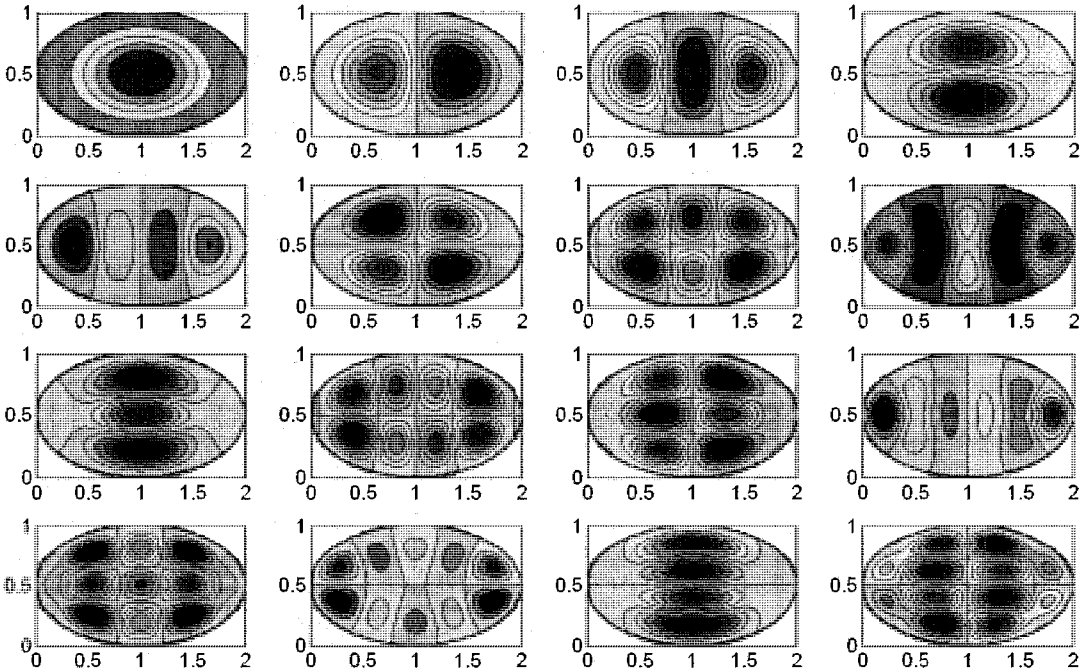

Fig. 39. Mode shape of elliptical plate $\alpha = 2$.

As shown in Fig. 39 the elliptical plates are grouped into the four categories as well, however, the rotation of the axis does not occur in this case since the plots are for elliptical plates and, unlike the circular case, the axis length varies with the angle.

Table 16: Comparison of the eigenvalues of reduced and full models of circular plates $\alpha = 1$.

Modes	Eigenvalues		Error (%)
	Reduced	Complete	
1	40.8633	40.8633	0
2	85.0419	85.0419	0
3	139.5849	139.5107	0.0532
4	140.6128	139.6302	0.7037
5	159.4812	159.2964	0.116
6	204.8935	204.8364	0.0279
7	272.418	204.8364	32.993
8	319.0803	245.6296	29.903
9	444.9232	280.2286	58.7715
10	649.3014	282.6517	129.7179

Table 17: Comparison of the eigenvalues of reduced and full model of elliptical plates $\alpha = 2$.

Modes	Eigenvalues		Error (%)
	Reduced	Complete	
1	109.5105	109.5105	0
2	157.9961	157.9961	0
3	225.2799	225.2799	0
4	279.4526	279.4498	0.001
5	312.1816	312.08	0.0326
6	353.0022	352.2941	0.201
7	460.3869	446.1932	3.1811
8	574.055	497.592	15.3666
9	850.1429	529.8696	60.4438
10	1544.98	556.711	177.5192

Table 16 and Table 17 show the comparison between the eigenvlaue, $\left(\omega a^2 \sqrt{\rho h / D}\right)$ of the reduced model and the complete model of circular and elliptical plates, respectively.

As shown, the reduction method succeded to aproximate half the number of the natural frequemcies of the reduced model with negligible error. Table 16 shows that this method has not shown the repeated eigenvalues of the (SA) and (AS) modes, while it has shown that of (AA) and (SS), are also repeated. Both are obtained by the calculation of the complete model. This is because the (SA) and (AS) modes are similar and thus the transformation deals with them as if they are one entity.

In conclusion, this chapter includes the reduction of generalized matrices where the DOFs do not form a physical coordinate system. A general method in terms of the generalized coordinates is used to obtain the natural frequencies of plates with arbitrary clamped supports. The reduction method showed its ability to approximate half of the reduced order model natural frequencies. Moreover this method is capable of eliminating duplicate modes while keeping repeated eigenvalues of different modes.

Chapter 6

Conclusions and recommendations for future work

6.1. Thesis summary

This thesis proposes a novel method for the model reduction of large discrete and continuous systems. To summarize the work covered in this study, the content of each chapter is briefly described.

Chapter 1 contains a brief historical review about FEM and Rayleigh-Ritz method. The basic formulation of the latter is explained. The use of BCOP as admissible functions was highlighted and a literature review of this technique for the solution of continuous structures is presented. Moreover Chapter 1 contains review of the model reduction methods presented in literature. The goal of extending the BCOP technique to reduce discrete models is mentioned.

In Chapter 2 the orthogonal vectors used for the model reduction are generated using Gram-Schmidt orthogonalization. This technique is applied on a discrete model of a building. This method has shown that it can approximate the eigenvalues of the complete model. However, this technique is cumbersome due the requirement of supplying the physical coordinates in order to generate the vectors.

Chapter 3 presents the formulation of static and exact dynamic condensation. The modified Gram-Schmidt and the static deflection methods to generate the boundary

characteristic orthogonal vectors are also proposed. The comparison between all the listed methods is done for the case of beams. It is shown that dynamic condensation will have zero error at all frequencies, however, the choice of slave and master DOFs may lead to the loss of some lower modes. Static condensation is poor for higher frequencies. The orthogonal vectors as static deflections has given good results with negligible error for more than half of the modes of the reduced order model. This method also obtains all the modes in proper sequence. Modified Gram-Schmidt method has shown the ability of overcoming the problem of dependent eigenvalues, however, it is cumbersome for use in complex structures.

Chapter 4 covers two case studies on which the newly proposed model reduction is applied. The first model consists of a hybrid continuous and discrete model of a city bus. The second model is a fluid filled coiled pipe heat exchanger. Both models are reduced and show good results. The frequency response analysis of the first model was done using different harmonic excitations to the exact and reduced models. The comparison shows negligible error but a large reduction in time. The second 3D model of the coiled pipe is reduced and the new method is successful in estimating the half of the reduced order model natural frequencies with negligible error.

Chapter 5 consists of the reduction of a generalized eigenvalue problem. The case of an elliptical plate is studied using the Rayleigh-Ritz method and two dimensional boundary characteristic orthogonal polynomials. The resulting generalized coordinate eigenvalue problem is reduced using a set of independent vectors.

6.2. Contributions

In this work a new reduction method, based on the use of boundary characteristic orthogonal polynomials in the Rayleigh-Ritz method on, is proposed. This method is mainly an extension of the BCOP method to discrete systems where it can be used as a reduction method. The major contributions are:

1. The generation of the boundary characteristic orthogonal vectors prevents any loss of modes.
2. The model reduction does not involve iterative steps without compromising the accuracy of the results.
3. The reduction procedure does not need neither the selection of master and slave degrees of freedom nor rearrangement of the matrices, and hence, the reduction procedure can be carried out even by beginners.
4. Time needed for harmonic analysis is reduced by orders of magnitude.

6.3. Major conclusions

Throughout this work a reduction method for multi degree of freedom systems is proposed. This method is based on the transformation of coordinates using a set of boundary characteristic orthogonal vectors as the transformation matrix. The advantages of this method can be summarized as:

1. Reduce the computation time required for obtaining the harmonic analysis.

The reduced order model is used to approximate the response due to harmonic excitation which has shown a good reduction in computation time. The economization in time is caused by the reduction of the size of the dynamic matrix that is required to obtain the response at each frequency. This enables us to reduce the step size of the frequency to get smother curves and better accuracy.

2. Elimination of recurrence procedure to compute the eigenvalues.

Unlike the exact dynamic condensation which is a recurrence method in which the frequency of interest is chosen and the calculated ones converge to the closest natural frequency, this method is not a recurrence method. The large error at the higher modes of the reduced order model, may be easily solved by increasing the number of employed vectors. Note that all the examples in this thesis have shown that secure results are obtained by employing the number of vectors to be double that of the desired number of frequencies.

3. No loss of lower modes and sequence is maintained.

Moreover, the sequence in the proposed method is exact. Resulting modes will appear in ascending sequence. This is an advantage because in other methods the sequence of modes may be destroyed because of an improper choice of master DOFS. Further, the duplicated modes are not shown in the reduced order model, however, the repeated modes are present. This is shown in Chapter 5 for the elliptical plates.

4. No need for the choice of master and slave degrees of freedom.

This method does not require the choice of master and slave DOFs, since the generalized coordinate are only the coefficients of the sum of the assumed deflection functions. In many different methods, complex analysis should be carried out in order to figure out the correct choice of master DOFs. Moreover, since no DOF are classified the FEM matrices do not need to be rearranged which also reduce the computational steps.

5. Does not require the coordinates in order to generate the transformation matrix.

One more advantage highlighted in this work is that the generation of the boundary characteristic orthogonal vectors as static deflections require neither modal nor physical coordinates as required in Gram-Schmidt orthogonalization.

6.4. Future work

This work presents a good method that combines simplicity and accuracy. More structures could be analyzed using this method in order to establish the suitability of the method for different types of structures. This method should be extended to substructuring for the case of repeated structure. Moreover, it has the potential to be used as a reduction method for different parts that would be assembled as reduced models. Also different method of accounting for the fluid mass can be used in order to study the effect of energy transferred from the fluid to the structure.

References

[1]. S. S. Rao, The Finite Element Method in Engineering, 2nd edition, Pergamon Press, (1989)

[2]. J. N. Reddy, An introduction to the finite element method, 3rd edition, Tata Mcgraw-Hill Publishing Company Limited, New Delhi, (2005)

[3]. W. T. Thomson and M. D. Dahleh, Theory of vibration with applications, 5th edition, Prentice Hall, (1997), pp. 363-365.

[4]. G. R. Kirchhoff, Uber das gleichgewicht und die bewegung einer elastischen scheibe, J. Math. (Crelle) 40, (1850).

[5]. W. Soedel, Vibration of shells and plates 3rd edition, Taylor & Francis e-Library, (2005).

[6]. S. M. Dickinson and E. K. H. Li, On the use of simply-supported plate functions in the Rayleigh-Ritz method applied to flexural vibration of rectangular plates, Journal of Sound and Vibration, 80, (1982), pp. 292-297.

[7]. D. Young, Vibration of rectangular plates by the Ritz method, Journal of Applied Mechanics, 17, (1950), pp. 448-453,

[8]. G. B. Warburton, The vibration of rectangular plates, proceedings of the Institution of Mechanical Engineers 168, (1954), pp. 371-384.

[9]. A. W. Leissa, Vibration of plates, (1969), NASA SP-160,

[10]. S. F. Bassily and S. M. Dickinson, Buckling and lateral vibration of rectangular plates subjected to in-plane loaded plates treated by a unified Ritz approach, Journal of Sound and Vibration 24, (1972), pp. 219-239.

[11]. A. W. Leissa, The free vibration of rectangular plates, Journal of Sound and Vibration 31, (1973), pp. 257-293.

[12]. S. M. Dickinson, The buckling and frequency of flexural vibration of rectangular plates using Rayleigh's method, Journal of Sound and Vibration 61, (1978), pp. 1-8.

[13]. R. B. Bhat, Natural frequency of rectangular plates using characteristic orthogonal polynomials In Rayleigh-Ritz method, Journal of Sound and Vibration 102 (4), (1985), pp. 493-499.

[14]. Richard L. Burden, J Douglas Faires and Albert C. Reynolds, Numerical analysis, 2nd edition, Prindle, Weber and Schmidt, Boston, Massachusetts, (1981).

[15]. Grossi R.O. and Bhat, R.B., A note on vibrating tapered beam, Journal of Sound and Vibration, 147(1), (1991), pp. 174-178.

[16]. R. B. Bhat, P. A. A. Laura, R. G. Gutierrez, V. H. Cortinez, and H. C. Sanzi, Numerical experiments on the determination of natural frequencies of transverse vibrations of rectangular plates of non-uniform thickness, Journal of Sound and Vibration, 138, (1990), pp. 205-219.

[17]. R. D. Belevins, Formulas for natural frequency and mode shape. New York, Van Nostrand Reinhold (1979).

[18]. R. O. Grossi, A. Aranda and R. B. Bhat, Vibration of tapered beams with one end spring hinged and the other end with tip mass, Journal of Sound and Vibration, 160(1), (1993), pp.175-178.

[19]. R. B. Bhat, Flexural vibration of polygonal plates using characteristic orthogonal polynomials in two variables, Journal of Sound and Vibration, 114, pp. 65-71, (1987).

[20]. A. W. Leissa and N. A. Jaber, Vibrations of completely free triangular plates, International Journal of Mechanical Science, 34(8), (1992), pp. 605-616.

[21]. B. Singh and V. Saxena, Transverse vibration of the triangular plates with variable thickness, Journal of Sound and Vibration, 194(4), (1996), pp. 471-496.

[22]. K. M. Liew and C. M. Wang, Vibration of triangular plates: point supports, mixed edges and partial internal curved supports, Journal of Sound and Vibration, 172(4), (1994), pp. 527-537.

[23]. K. M. Liew, On the use of pb-2 Rayleigh-Ritz method for flexural vibration of triangular plates with curved internal support, Journal of Sound and Vibration, 165(2), (1993), pp. 329-340.

[24]. C. Rajalingham and R. B. Bhat, Axisymmetric vibration of circular plates and its analog in elliptical plates using characteristic orthogonal polynomials, Journal of Sound and Vibration, 161(1), (1993), pp. 109-118.

[25]. C. Rajalingham and R.B. Bhat, Vibration of elliptic plates using characteristic orthogonal polynomials in Rayleigh-Ritz method, International Journal of Mechanical Sciences, 33, (1991), pp. 705-716.

[26]. B. Singh and S. Chakraverty, Transverse vibration of simply-supported elliptic and circular plates using orthogonal polynomials, Journal of Sound and Vibration, 1733(9), (1994), pp. 289-299.

[27]. R. B. Bhat, Application of Rayleigh-Ritz method on the finite element model of a structure as a means of co-ordinate reduction, Journal of Sound and Vibration, 108(2), (1986), pp. 355-356.

[28]. R. J. Alkhoury and R. B. Bhat, Model reduction using orthogonal vector set for multi degree of freedom vibrating systems, CSME forum, Ottawa, (2008).

[29]. H. J. Staib, An alternative to Gram-Schmidt process, Mathematics Magazine, 42(4), (1969), pp. 203-205.

[30]. R. J. Guyan, Reduction of stiffness and mass matrices, AIAA Journal, 280(3), (1965), pp. 171-175.

[31]. B. M. Irons, Structural eigenvalue problem: elimination of unwanted variables. AIAA Journal, 3, (1965), pp. 961-962.

[32]. J. C. O'Callahan, A procedure for an improved reduced system (IRS) model, Proceedings of the 7th International modal analysis conference, Las Vegas, (1989).

[33]. P. Salvini and F. Vivio, Dynamic reduction strategies to extend modal analysis approach at higher frequencies, Finite Element in Analysis and Design, 43, (2007), pp. 931-940.

[34]. Y. T. Leung, An accurate method of dynamic condensation in structural vibration analysis, International Journal for Numerical Method in Engineering, 12, (1978), pp.1705-1715.

[35]. L. I. Mikelbust, B. Skallerud and T. Rolvag, On deficiencies in model reduction in nonlinear dynamic problems. Euromech Colloquium on identification and updating methods for mechanical structures, Praha, (2002).

[36]. L. I. Myklebust and B. Skallerud, Model reduction methods for flexible Structures, proceedings of the 15th Nordic Seminar on Computational Mechanics, Aalborg, Denmark, (2002), pp. 18-19.

[37]. W. C. Hurty, J. D. Collins and G. C. Hart, Dynamic analysis of large structures by modal synthesis techniques, Computers and Structures, 1(4), (1971), pp. 535-563.

[38]. R. R. Craig and M. C. C. Bampton. Coupling of substructures in dynamic analysis, AIAA Journal, 6(7), (1968), pp. 1313-1319.

[39]. W. A. Benfield and R. F. Hruda, Vibration analysis of structures by component mode substitution, AIAA Journal, 9(7), (1971), pp. 1255-1261.

[40]. X. Lu, Y. Chen, J. Chen, Dynamic substructure analysis of structures using Lanczos vector, 1st world congress in computational mechanics, Austin Texas, (1986).

[41]. C. Lanczos, An iterative method for the solution of the eigenvalue problem of linear differential and integral operators, Journal of Research of National Bureau of Standards, 45(4), (1950), pp. 255-282.

[42]. P. Leger, E. L. Wilson and R. W. Clough, The use of load dependant vectors for dynamic and earthquake analysis, report no. UCB/EERC 86-04, Earthquake Engineering Research Center, University of California, Berkeley, California, (1986).

[43]. H. Xia and J. L. Humar, Frequency dependent Ritz vectors, Earthquake Engineering & Structural Dynamics, 21(3), (1992), pp. 215-231.

[44]. L. Meirovitch, Computational method in structural dynamics, Sijthoff & Noordhoff, Alphen aan den Rijn, The Netherlands, Rockville, Maryland, U.S.A, (1980), pp. 373-380.

[45]. A. Y. T. Leung, Dynamic stiffness and substructures, Springer-Verlag, London Limited, (1993).

[46]. T. T. Soong and G. F. Dargush, Passive energy dissipation systems in structural engineering, Wiley Publications, Chichester, (1997).

[47]. M. C. Constantinou and I. G.Tadjbakhsh, Optimum design of a first story damping system, Computers and Structures, 17 (2), (1983), pp. 305-310.

[48]. G. D. Hahn and K. R. Sathiavageeswaran, Effects of added-damper distribution on the seismic response of buildings, Computers and Structures, 43 (5), (1992), pp. 941-950.

[49]. O. Lavan and R. Levy, Optimal design of supplemental viscous dampers for linear framed structures, Earthquake Engineering and Structural Dynamic, 35, (2006), pp. 337-356.

[50]. S. Narasimhan and S. Nagarajaiah, Smart base isolated buildings with variable friction systems: H∞ controller and SAIVF device, Earthquake Engineering and Structural Dynamics, 35, (2006), pp. 921-942.

[51]. T. H. Richards, A. Y. T. Leung, An accurate method in structural vibrating analysis, Journal of Sound and Vibration 55, (1977), pp. 363-376.

[52]. R. B. Bhat, Effect of normal mode components in the assumed deflection shapes in Rayleigh-Ritz method, Journal of Sound and Vibration, 189(4), (1996), pp. 407-419.

[53]. Y. Wan and J. M. Schimmels, Improved vibration isolating seat suspension designs based on position dependent nonlinear stiffness and damping characteristics, ASME transactions, 125, (2003), pp. 331-338.

[54]. V. K. Tewari and N. Prasad, Three-DOF modeling of tractor seat-operator system, Journal of Terramechanics, 36, (1999), pp. 207-219.

[55]. T. Gunston, An investigation of suspension seat damping using a theoretical model, Proceeding of the 35th Meeting of the U.K. Group on Human Response to Vibration, (2000), pp. 137-149.

[56]. V. Kumar, M. Mirdha, A. K. Gupta and K. D. P. Nigam, Coiled flow as a heat exchanger, Chemical Engineering Science, 62, (2007), pp. 2386-2396.

Appendix-A

Consider the system of equation shown in the following equation:

$$[B]\{x\} = [I]\{y\} \tag{A.1}$$

where, $[I]$ is the identity matrix. Performing a set of row operation on both sides of the equation (A.1) results in the following where A is the desired matrix:

$$[T]\{x\} = [A]\{y\} \tag{A.2}$$

Multiplying equation (A.2) by $[T]^{-1}$ to obtain the following:

$$[I]\{x\} = [T]^{-1}[A]\{y\} \tag{A.3}$$

In the same time from equations (A.1) it is easily seen that:

$$[I]\{x\} = [B]^{-1}\{y\} \tag{A.4}$$

Combining equations (A.3) and (A.4) results in the following equation:

$$[T]^{-1}[A] = [B]^{-1} \tag{A.5}$$

Multiplying the previous equation by $[B]$ and rearranging it to obtain:

$$[T]^{-1}[A][B] = [I] \tag{A.6}$$

Then we can write that:

$$[A][B]=[T] \tag{A.7}$$

The next task is to use equation (A.7) in order to prove that the matrix $[A]$ holds the desired properties and that $[D]=[A][B][A]^T$ is diagonal. To achieve that, we will prove that D is both symmetric and an upper triangular matrix in the same time.

First, the goal is to show that $[A][B][A]^T$ is symmetric, knowing that $[B]$ is also symmetric.

$$[D]=[D]^T \tag{A.8}$$

To prove equation (A.8) we will find what is $[D]^T$ equal to

$$[D]^T=\left([A][B][A]^T\right)^T \tag{A.9}$$

or,

$$[D]^T=[A][B]^T[A]^T \tag{A.10}$$

Since $[B]$ is symmetric, equation (A.10) can be written as follows:

$$[D]^T=[A][B][A]^T=[D] \tag{A.11}$$

At this level it is proven that $[D]$ is symmetric. The second step is to prove that $[D]$ is an upper triangular matrix.

Substituting equation (A.7) in equation (A.11) yields:

$$[D]^T = [A][B][A]^T = [T][A]^T \tag{A.12}$$

Since, $[T]$ and $[A]^T$ are upper triangular matrices, $[D]$ is also upper triangular. Being proved that $[D]$ is also symmetric then it is clear that this matrix is diagonal.